

Hamiltonian simulation using quantum singular value transformation: complexity analysis and application to the linearized Vlasov-Poisson equation

Kiichiro Toyoizumi,¹ Naoki Yamamoto,^{1, 2} and Kazuo Hoshino¹

¹*Department of Applied Physics and Physico-Informatics,*

Keio University, Hiyoshi 3-14-1, Kohoku-ku, Yokohama, 223-8522, Japan

²*Quantum Computing Center, Keio University, Hiyoshi 3-14-1, Kohoku-ku, Yokohama, 223-8522, Japan*

Quantum computing can be used to speed up the simulation time (more precisely, the number of queries of the algorithm) for physical systems; one such promising approach is the Hamiltonian simulation (HS) algorithm. Recently, it was proven that the quantum singular value transformation (QSVT) achieves the minimum simulation time for HS. An important subroutine of the QSVT-based HS algorithm is the amplitude amplification operation, which can be realized via the oblivious amplitude amplification or the fixed-point amplitude amplification in the QSVT framework. In this work, we execute a detailed analysis of the error and number of queries of the QSVT-based HS and show that the oblivious method is better than the fixed-point one in the sense of simulation time. Based on this finding, we apply the QSVT-based HS to the one-dimensional linearized Vlasov-Poisson equation and demonstrate that the linear Landau damping can be successfully simulated.

I. INTRODUCTION

A. Background

Quantum computers are expected to outperform classical counterparts in some problems. Several quantum algorithms have obtained speedups over classical ones, such as the Grover search algorithm [1], Shor's algorithm for integer factorization [2], and the HHL algorithm [3, 4]. Quantum computing also gives us algorithms for solving physics problems. In particular, the algorithms [5, 6] realize exponential speedup for the simulation of quantum systems. This seems natural since quantum computing is based on quantum mechanics. In recent years, some quantum algorithms for simulating classical physical systems have been developed, such as the Navier-Stokes equation [7, 8], plasma equations [9–12], the Poisson equation [13, 14], and the wave equation [15, 16].

One of the quantum algorithms for simulating physical systems is a Hamiltonian simulation (HS) algorithm [17–26], which implements $U = \exp(-iHt)$, where H is a time-independent Hamiltonian and t is an evolution time. The optimal HS result was shown by Low and Chuang using quantum signal processing (QSP) [27, 28]. This result has been generalized to the quantum singular value transformation (QSVT) in Ref. [29]. QSVT is a quantum algorithm for applying a polynomial transformation $P^{(SV)}(A)$ to the singular values of a given matrix A , called the singular value transformation. Notably, QSVT can formulate major quantum algorithms in a unified way, such as the Grover search, phase estimation [30], matrix inversion, quantum walks [31], and HS algorithm. Therefore, QSVT is called a grand unification of quantum algorithms in Ref. [32].

The HS algorithm using QSVT has been proposed in Refs. [29, 32]. The algorithm includes an amplitude amplification algorithm that can be implemented by QSVT as a subroutine. There are two QSVT-based amplitude amplification algorithms proposed for HS; one is the

oblivious amplitude amplification (OAA) algorithm [29], and the other is the fixed-point amplitude amplification (FPAA) algorithm [32]. However, there have been no discussion to compare those two schemes from neither theoretical nor numerical viewpoints. It would be helpful to clarify which one is preferable when the QSVT-based HS algorithm is applied to physical systems.

B. Contribution of this paper

We elaborate the QSVT-based HS using explicit quantum circuits and discuss the approximation error and query complexity. As a result, the number of queries for the OAA-based HS scales as $\mathcal{O}(t + \log(1/\varepsilon))$, whereas the FPAA-based one scales as $\mathcal{O}(t \log(1/\varepsilon) + \log^2(1/\varepsilon))$, where t is an evolution time and ε is an error tolerance. To support this fact, we perform numerical experiments: we plot the number of queries for a wide range of parameters t and ε ; we curve-fit the data to identify the constant factors and coefficients of the number of queries hidden behind the asymptotic scalings. Our findings indicate that the OAA-based method is both theoretically and numerically advantageous than the FPAA-based method in the sense of the number of queries. Importantly, this advantage is consistent, independent of the type of the Hamiltonian.

To demonstrate the effectiveness of the QSVT-based HS combined with the above-described detailed analysis, we apply the OAA-based HS to the simulation of the linearized Vlasov-Poisson system. This system can be transformed into the same form of the unitary time evolution of quantum systems [9]. In addition to the simulation, we discuss several issues unaddressed in previous studies on quantum algorithms for plasma simulation [9–12]: We discuss the computational complexity of extending evolution time using sequential short HS circuits; we propose an algorithm to obtain a quantity related to the distribution function; we provide explicit quantum cir-

cuits for the higher dimensional systems. Furthermore, we show a potential advantage of applying HS to physical systems compared to the classical Euler method.

C. Comparison to prior work

The QSVT-based HS algorithms have been introduced in Refs. [29, 32]. The authors of Ref. [29] have originally proposed the QSVT framework. Within the framework, they developed a method for implementing the exponential function and the OAA algorithm, which constructs the Chebyshev polynomial of the first kind. Combining these methods, they have realized QSVT-based HS and shown that its asymptotic complexity is consistent with the result of HS by Low and Chuang [27, 28], known to be optimal. The authors of Ref. [32] have reviewed that several major quantum algorithms can be described in a unified way within the QSVT framework and suggested for HS the use of FPAA, which constructs the approximate polynomial of the sign function. These authors have independently proposed using OAA and FPAA for HS, respectively, with rough analyses of the approximation error and query complexity. However, a theoretical or numerical comparison of these methods remains absent.

To our knowledge, no investigation exists to compare OAA and FPAA in a non-QSVT framework. This is probably because these algorithms have been originally developed for distinct purposes. The OAA algorithm has been initially developed to simulate a sparse Hamiltonian evolution [21, 23], achieving amplitude amplification without the reflection operator about an unknown initial state. It is also used to decompose single-qubit unitaries [33] and compute matrix products for non-unitary matrices [34]. On the other hand, the FPAA algorithm is an algorithm that ensures amplitude amplification regardless of an unknown amplitude. Notably, several non-QSVT-based FPAA algorithms have been developed, such as the $\pi/3$ -algorithm [35], the measurement-based algorithm [36], and the FPAA technique by Yoder et al. [37].

Several studies have addressed quantum algorithms for plasma simulations. The authors of Ref. [10] have conducted an extensive survey on applying quantum computers to plasma simulations. The authors of Ref. [9] have introduced the quantum algorithm for calculating the time evolution of the one-dimensional linearized Vlasov-Poisson system using the HS algorithm by Low and Chuang [27, 28]. They have concluded that the algorithm achieves exponential speedup for a velocity grid size. They have also discussed an estimation of the electric field with the quantum amplitude estimation algorithm [38] and simulated its linear Landau damping. While the state's amplitude comprises the electric field and the distribution function, no method has been proposed to extract the latter's quantity from the state. They have indicated that the above findings can be extended to systems with higher dimensions,

yet without providing explicit circuits. The authors of Ref. [12] have examined the computational complexity for a system size, of a quantum algorithm for the one-dimensional Vlasov-Poisson system with collisions. They have adopted the Hermite representation, reducing the equations to a linear ODE problem—distinct from our work and Ref. [9]. The authors of Ref. [11] have implemented the HS algorithm for one-dimensional cold plasma waves, dividing the HS circuit into shorter circuits to avoid a large evolution time t , yet without discussing its cost.

D. Organization of the paper

The rest of this paper is organized as follows. In Sec. II we present a brief description of QSVT with application to the trigonometric functions; then we show the transformation from the linearized Vlasov-Poisson system to a form of the Schrödinger equation. We discuss the error and query complexity of QSVT-based HS in Sec. III. The quantum algorithm for the linearized Vlasov-Poisson system is discussed in Sec. IV. We show the numerical results in Sec. V. The paper is then concluded in Sec. VI.

II. PRELIMINARY

A. Quantum singular value transformation

Quantum singular value transformation (QSVT) [29, 32] is a quantum algorithm for applying a polynomial transformation $P^{(SV)}(A)$ to the singular values of a given matrix A . As mentioned above, QSVT has been applied to many problems, including HS. In these problems, a degree- d polynomial P_ε is used to ε -approximate the corresponding objective function P . How much quantum speedup is obtained depends on the degree d . Recall that QSVT generalizes the result of QSP [27, 28, 39, 40]. We present a brief description of the derivation from QSP to QSVT in Appendix A.

We introduce the block-encoding [29], which represents a matrix A as the upper-left block of a unitary matrix U . Let A be a matrix acting on s qubits, U be a unitary matrix acting on $a+s$ qubits. Then, for $\alpha > 0$ and $\varepsilon > 0$, U is called an (α, a, ε) -block-encoding of A , if

$$\|A - \alpha(\langle 0|_a \otimes I)U(|0\rangle_a \otimes I)\| \leq \varepsilon, \quad (1)$$

where $|0\rangle_a = |0\rangle^{\otimes a}$. Note that, since $\|U\| = 1$, we necessarily have $\|A\| \leq \alpha + \varepsilon$. If $\varepsilon = 0$, then we can represent A as the upper-left block of U :

$$U = \begin{bmatrix} A & \cdot \\ \alpha & \cdot \\ \cdot & \cdot \end{bmatrix}, \quad (2)$$

where the dot \cdot denotes a matrix with arbitrary elements.

Recall now that the singular value decomposition of A ; that is, any matrix $A \in \mathbb{C}^{m \times n}$ can be decomposed as

$$A = W\Sigma V, \quad (3)$$

where $W \in \mathbb{C}^{m \times m}$ and $V \in \mathbb{C}^{n \times n}$ are unitary matrices; Σ is diagonal and contains the set of non-negative real numbers $\{\sigma_k\}$, called the singular values of A . The matrix A is also expressed as

$$A = \sum_{k=1}^r \sigma_k |w_k\rangle \langle v_k|, \quad (4)$$

where $\{|w_k\rangle\}$ and $\{|v_k\rangle\}$ are right and left singular vectors, and $r = \text{rank}(A)$.

The singular value transformation is defined from the singular value decomposition as follows: for an odd polynomial $P \in \mathbb{C}$,

$$P^{(\text{SV})}(A) \equiv \sum_k P(\sigma_k) |w_k\rangle \langle v_k|, \quad (5)$$

and for an even polynomial $P \in \mathbb{C}$,

$$P^{(\text{SV})}(A) \equiv \sum_k P(\sigma_k) |v_k\rangle \langle v_k|. \quad (6)$$

If A is Hermitian and positive semidefinite, then $P^{(\text{SV})}(A)$ is equal to the eigenvalue transformation $P(A)$.

Suppose that U is an $(\alpha, a, 0)$ -block-encoding of A as in Eq. (2). Then, a unitary matrix U_Φ called the alternating phase modulation sequence in Ref. [29] is defined as follows: for odd d ,

$$U_\Phi \equiv e^{i\phi_0\Pi} U e^{i\phi_1\Pi} \prod_{k=1}^{(d-1)/2} (U^\dagger e^{i\phi_{2k}\Pi} U e^{i\phi_{2k+1}\Pi}), \quad (7)$$

and for even d ,

$$U_\Phi \equiv e^{i\phi_0\Pi} \prod_{k=1}^{d/2} (U^\dagger e^{i\phi_{2k-1}\Pi} U e^{i\phi_{2k}\Pi}), \quad (8)$$

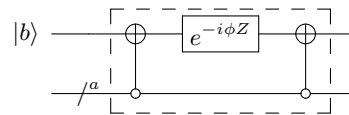
where $\Phi = \{\phi_0, \phi_1, \dots, \phi_a\} \in \mathbb{R}^{d+1}$ is called the *phases* and $\Pi = 2|0\rangle_a \langle 0| - I$. The unitary matrix $\exp(i\phi\Pi)$ can be implemented as in Fig. 1. The phases are calculated efficiently from the degree- d polynomial P on a classical computer. The details of the calculation can be found in Refs. [29, 41]. In this work, we use the code provided in Ref. [42] to calculate the phases.

Given a degree- d polynomial $P \in \mathbb{C}$ and the corresponding phases $\Phi \in \mathbb{R}^{d+1}$, the unitary U_Φ can be represented as a $(1, a, 0)$ -block-encoding of $P^{(\text{SV})}(A/\alpha)$:

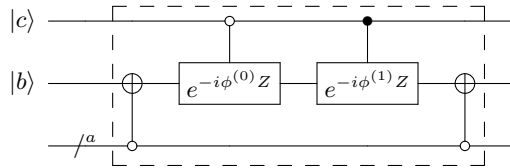
$$U_\Phi = \begin{bmatrix} P^{(\text{SV})} \left(\frac{A}{\alpha} \right) & \cdot \\ \cdot & \cdot \end{bmatrix}, \quad (9)$$

$$P^{(\text{SV})} \left(\frac{A}{\alpha} \right) = (\langle 0|_a \otimes I) U_\Phi (|0\rangle_a \otimes I).$$

Note that P is not arbitrary and has some constraints. P satisfies the following conditions [29, 32]:



(a) $|b\rangle \langle b| \otimes e^{(-1)^b i\phi\Pi}$



(b) $|cb\rangle \langle cb| \otimes e^{(-1)^b i\phi^{(c)}\Pi}$

FIG. 1: Quantum circuits used to implement the unitary matrix $\exp(i\phi\Pi)$. In Fig. 1(a), a single phase ϕ is used, and the series of gates surrounded by dashed lines is denoted by $S_1(\phi)$, which is used in Fig. 3 and 4. In Fig. 1(b), two phases $\phi^{(0)}$ and $\phi^{(1)}$ are used, and the series of gates surrounded by dashed lines is denoted by $S_2(\phi^{(0)}, \phi^{(1)})$, which is used in Fig. 2.

- (i) P has parity $d \bmod 2$
- (ii) $\forall x \in [-1, 1] : |P(x)| \leq 1$
- (iii) $\forall x \in (-\infty, -1] \cup [1, \infty) : |P(x)| \geq 1$
- (iv) if d is even, then $\forall x \in \mathbb{R} : P(ix)P^*(ix) \geq 1$.

These conditions are complicated, but taking the real part of P relaxes them. That is, $P_{\Re} \equiv \text{Re}(P)$ satisfies the following conditions:

- (v) P_{\Re} has parity $d \bmod 2$
- (vi) $\forall x \in [-1, 1] : |P_{\Re}(x)| \leq 1$,

and the corresponding phases can be calculated by [29, 32]

B. Applying QSVT to trigonometric functions

Let U be a $(1, a, 0)$ -block-encoding of H :

$$U = \begin{bmatrix} H & \cdot \\ \cdot & \cdot \end{bmatrix}, \quad H = (\langle 0|_a \otimes I) U (|0\rangle_a \otimes I), \quad (10)$$

where $\|H\| \leq 1$ is a Hermitian matrix that is positive semidefinite. We will discuss later the case H is negative and normalized by α . The goal of HS is to construct a quantum circuit U_{HS} that is a block-encoding of $\exp(-iHt)$ using the unitary U , where t is a evolution time. Note that U_{HS} cannot be realized single U_Φ using QSVT, because $\exp(-ixt)$ has no definite parity. To avoid this problem, one can instead apply QSVT to two different functions: $\cos(xt)$ and $\sin(xt)$.

The functions $\cos(xt)$ and $\sin(xt)$ are given by the Jacobi-Anger expansion:

$$\cos(xt) = J_0(t) + 2 \sum_{k=1}^{\infty} (-1)^k J_{2k}(t) T_{2k}(x), \quad (11)$$

$$\sin(xt) = 2 \sum_{k=0}^{\infty} (-1)^k J_{2k+1}(t) T_{2k+1}(x), \quad (12)$$

where $J_m(t)$ is the m -th Bessel function of the first kind and $T_k(x)$ is the k -th Chebyshev polynomial of the first kind. One can obtain ε_{tri} -approximation to $\cos(xt)$ and $\sin(xt)$ by truncating Eqs. (11) and (12) at an index R :

$$\left| \cos(xt) - J_0(t) - 2 \sum_{k=1}^R (-1)^k J_{2k}(t) T_{2k}(x) \right| \leq \varepsilon_{\text{tri}}, \quad (13)$$

$$\left| \sin(xt) - 2 \sum_{k=0}^R (-1)^k J_{2k+1}(t) T_{2k+1}(x) \right| \leq \varepsilon_{\text{tri}}, \quad (14)$$

where $0 < \varepsilon_{\text{tri}} < 1/e$ and

$$R(t, \varepsilon_{\text{tri}}) = \left\lfloor \frac{1}{2} r \left(\frac{et}{2}, \frac{5}{4} \varepsilon_{\text{tri}} \right) \right\rfloor, \quad (15)$$

$$r(t, \varepsilon_{\text{tri}}) = \Theta \left(t + \frac{\log(\frac{1}{\varepsilon_{\text{tri}}})}{\log(e + \log(\frac{1}{\varepsilon_{\text{tri}}})/t)} \right) \leq \mathcal{O}(t + \log(1/\varepsilon_{\text{tri}})). \quad (16)$$

For more details see Ref. [29].

We denote the approximate polynomials of Eqs. (13) and (14) by $P_{\varepsilon_{\text{tri}}}^{\cos}(x)$ and $P_{\varepsilon_{\text{tri}}}^{\sin}(x)$. Since cosine and sine are bounded in magnitude by 1, these polynomials obey $|P_{\varepsilon_{\text{tri}}}^{\cos}(x)|, |P_{\varepsilon_{\text{tri}}}^{\sin}(x)| \leq 1 + \varepsilon_{\text{tri}}$. Therefore, the condition (vi) is violated. Here, we introduce rescaled polynomials

$$P_{\varepsilon_{\text{tri}}, \kappa}^{\cos}(x) = \kappa P_{\varepsilon_{\text{tri}}}^{\cos}(x), \quad P_{\varepsilon_{\text{tri}}, \kappa}^{\sin}(x) = \kappa P_{\varepsilon_{\text{tri}}}^{\sin}(x), \quad (17)$$

where $\kappa = 1/(1 + \varepsilon_{\text{tri}})$. These polynomials satisfy the following inequality:

$$\begin{aligned} & \left| \frac{\kappa}{2} e^{-ixt} - \frac{P_{\varepsilon_{\text{tri}}, \kappa}^{\cos}(x) - iP_{\varepsilon_{\text{tri}}, \kappa}^{\sin}(x)}{2} \right| \\ & \leq \frac{1}{2} |\kappa \cos(xt) - P_{\varepsilon_{\text{tri}}, \kappa}^{\cos}(x)| + \frac{1}{2} |\kappa \sin(xt) - P_{\varepsilon_{\text{tri}}, \kappa}^{\sin}(x)| \\ & \leq \frac{\kappa \varepsilon_{\text{tri}} + \kappa \varepsilon_{\text{tri}}}{2} = \kappa \varepsilon_{\text{tri}}, \end{aligned} \quad (18)$$

where in the first inequality we used the triangle inequality.

Suppose the phases $\Phi^{(c)} \in \mathbb{R}^{2R+1}$ and $\Phi^{(s)} \in \mathbb{R}^{2R+2}$ are calculated from the $2R$ -th polynomial $P_{\varepsilon_{\text{tri}}, \kappa}^{\cos}(x)$ and $(2R+1)$ -th polynomial $P_{\varepsilon_{\text{tri}}, \kappa}^{\sin}(x)$. The quantum circuit U_{exp} using these phases is shown in Fig. 2. This circuit constructs the $(1, a+2, \kappa \varepsilon_{\text{tri}})$ -block-encoding of $\kappa e^{-iHt}/2$:

$$\left\| \frac{\kappa}{2} e^{-iHt} - (|0\rangle_{abc} \otimes I) U_{\text{exp}} (|0\rangle_{abc} \otimes I) \right\| \leq \kappa \varepsilon_{\text{tri}}, \quad (19)$$

with R uses of U and U^\dagger , and one use of the controlled- U . Therefore, the query complexity of U_{exp} is

$$R + R + 1 = 2 \left\lfloor \frac{1}{2} r \left(\frac{et}{2}, \frac{5}{4} \varepsilon_{\text{tri}} \right) \right\rfloor + 1 \quad (20)$$

$$\leq \mathcal{O}(t + \log(1/\varepsilon_{\text{tri}})). \quad (21)$$

To obtain the block-encoding of $\exp(-iHt)$, the amplitude amplification must be used. In Sec. III, we discuss two types of the QSVT-based amplitude amplification algorithms: the oblivious amplitude amplification (OAA) [29] and fixed-point amplitude amplification (FPAA) [32].

C. The linearized Vlasov-Poisson system

The time evolution of the distribution function $f(\mathbf{x}, \mathbf{v}, t)$ for electrons with stationary ions and the electric field $\mathbf{E} = (E_x, E_y, E_z)$ governed by the Vlasov-Poisson system is described by the following equations:

$$\frac{\partial f}{\partial t} + \mathbf{v} \cdot \nabla f - \frac{e}{m} \mathbf{E} \cdot \frac{\partial f}{\partial \mathbf{v}} = 0, \quad (22)$$

$$\frac{\partial \mathbf{E}}{\partial t} = \frac{1}{\varepsilon_0} \int e \mathbf{v} f d\mathbf{v}, \quad (23)$$

where e is the absolute value of the electron charge, m is the electron mass, and ε_0 is the permittivity of the vacuum. The variables f and \mathbf{E} are expanded into the equilibrium terms (labeled by 0) and perturbations (labeled by 1) to linearize Eq. (22):

$$\begin{aligned} f(\mathbf{x}, \mathbf{v}, t) &= f_0(\mathbf{v}) + f_1(\mathbf{x}, \mathbf{v}, t), \\ \mathbf{E} &= \mathbf{E}_1(\mathbf{x}, t). \end{aligned} \quad (24)$$

Note that we do not deal with the case when the nonzero electric field \mathbf{E}_0 increases the system's energy, i.e., $\mathbf{E}_0 = 0$.

We assume a Maxwellian background distribution $f_0 = f_M$ and apply the same transformations as in Ref. [9]: a Fourier transformation of the variables in space, change of variables, and discretization in velocity space with the following dimensionless variables:

$$\begin{aligned} \hat{\mathbf{k}} &= \lambda_{D_e} \mathbf{k}, \quad \hat{t} = \omega_{pe} t, \quad \hat{\mathbf{v}} = \frac{\mathbf{v}}{\lambda_{D_e} \omega_{pe}}, \\ \hat{f} &= \frac{(\lambda_{D_e} \omega_{pe})^3}{n_e} f, \quad \hat{\mathbf{E}} = \frac{e \lambda_{D_e}}{k_B T_e} \mathbf{E}, \end{aligned} \quad (25)$$

where $\mathbf{k} = (k_x, k_y, k_z)$ is the wave vector for the Fourier transformation, λ_{D_e} is the Debye length with ions neglected, ω_{pe} is the electron plasma frequency, n_e is the electron number density, T_e is the electron temperature, and k_B is the Boltzmann constant. As a result, Eqs. (22)

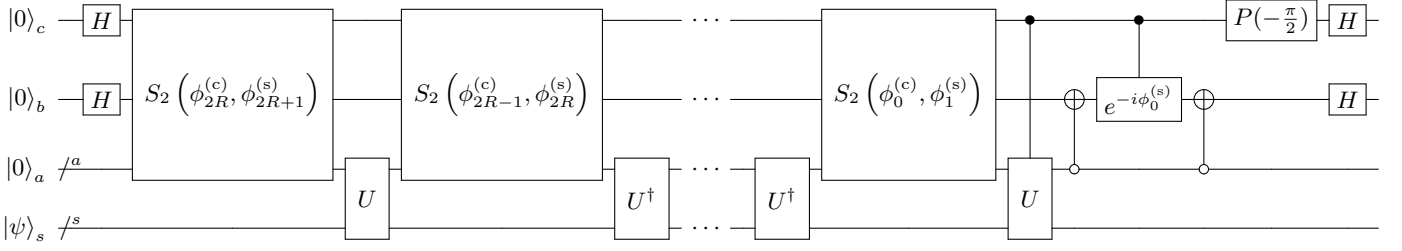


FIG. 2: Quantum circuit U_{exp} that is a $(1, a + 2, \kappa \varepsilon_{\text{tri}})$ -block-encoding of $\kappa \exp(-iHt)/2$. The gate S_2 is shown in Fig. 1(b), the unitary U is given by Eq. (10), and the phases $\Phi^{(c)} \in \mathbb{R}^{2R+1}$ and $\Phi^{(s)} \in \mathbb{R}^{2R+2}$ are calculated from the $2R$ -th polynomial $P_{\varepsilon_{\text{tri}}, \kappa}^{\text{cos}}(x)$ and $(2R + 1)$ -th polynomial $P_{\varepsilon_{\text{tri}}, \kappa}^{\text{sin}}(x)$ in Eq. (17), where R is given by Eq. (15).

and (23) becomes

$$\frac{dF_j}{dt} = -i(k_x v_{j_x} + k_y v_{j_y} + k_z v_{j_z}) F_j - i\mu_j (v_{j_x} E_x + v_{j_y} E_y + v_{j_z} E_z), \quad (26)$$

$$\frac{dE_p}{dt} = -i \sum_j \mu_j v_{j_p} F_j \quad (p = x, y, z), \quad (27)$$

where the subscripts 1 have been dropped,

$$\mu_j = \mu(v_{j_x}, v_{j_y}, v_{j_z}) = \sqrt{\Delta v f_M(v_{j_x}, v_{j_y}, v_{j_z})}, \quad (28)$$

$$F_j = F(v_{j_x}, v_{j_y}, v_{j_z}, t) = i \sqrt{\frac{\Delta v}{f_M(v_{j_x}, v_{j_y}, v_{j_z})}} f(v_{j_x}, v_{j_y}, v_{j_z}, t), \quad (29)$$

$$\sum_j \cdot = \sum_{j_x=0}^{N_{v_x}-1} \sum_{j_y=0}^{N_{v_y}-1} \sum_{j_z=0}^{N_{v_z}-1} \cdot, \quad (30)$$

where $\Delta v = \Delta v_x \Delta v_y \Delta v_z$ is the product of the mesh sizes, $N_{v_x} = 2^{n_{v_x}}$, $N_{v_y} = 2^{n_{v_y}}$ and $N_{v_z} = 2^{n_{v_z}}$ are the grid sizes in velocity space, and the velocity space grid is represented by index $\mathbf{j} = (j_x, j_y, j_z)$.

Equations (26) and (27) can be rewritten in a form of the Schrödinger equation:

$$\frac{d|\psi(t)\rangle}{dt} = -iH|\psi(t)\rangle, \quad (31)$$

where H is a time-independent Hamiltonian and $|\psi(t)\rangle$ is a quantum state whose amplitudes are the variables, which is written in bra-ket notation as

$$|\psi(t)\rangle = \frac{1}{\eta} \left(\sum_j F_j |0\rangle_r |\mathbf{j}\rangle_v + E_x |1\rangle_r |\mathbf{0}\rangle_v + E_y |2\rangle_r |\mathbf{0}\rangle_v + E_z |3\rangle_r |\mathbf{0}\rangle_v \right), \quad (32)$$

where $|\mathbf{j}\rangle_v = |j_x\rangle_{v_x} |j_y\rangle_{v_y} |j_z\rangle_{v_z}$, $|\mathbf{0}\rangle_v = |0\rangle_{v_x} |0\rangle_{v_y} |0\rangle_{v_z}$ and the normalization constant

$$\eta = \sqrt{\sum_j |F_j|^2 + |E_x|^2 + |E_y|^2 + |E_z|^2}. \quad (33)$$

$|\psi(t)\rangle$ has two registers labeled by r and v . The r register encodes the variable index: $|0\rangle_r \leftrightarrow F$, $|1\rangle_r \leftrightarrow E_x$, $|2\rangle_r \leftrightarrow E_y$ and $|3\rangle_r \leftrightarrow E_z$. The v register stores the velocity space dependence of F : $|0\rangle_r |\mathbf{j}\rangle_v \leftrightarrow F_j$. The corresponding Hamiltonian H , which acts on these registers, is given by

$$H = \sum_j \left[(k_x v_{j_x} + k_y v_{j_y} + k_z v_{j_z}) |0\rangle_r |\mathbf{j}\rangle_v \langle 0|_r \langle \mathbf{j}|_v + \mu_j v_{j_x} (|0\rangle_r |\mathbf{j}\rangle_v \langle 1|_r \langle \mathbf{0}|_v + |1\rangle_r |\mathbf{0}\rangle_v \langle 0|_r \langle \mathbf{j}|_v) + \mu_j v_{j_y} (|0\rangle_r |\mathbf{j}\rangle_v \langle 2|_r \langle \mathbf{0}|_v + |2\rangle_r |\mathbf{0}\rangle_v \langle 0|_r \langle \mathbf{j}|_v) + \mu_j v_{j_z} (|0\rangle_r |\mathbf{j}\rangle_v \langle 3|_r \langle \mathbf{0}|_v + |3\rangle_r |\mathbf{0}\rangle_v \langle 0|_r \langle \mathbf{j}|_v) \right]. \quad (34)$$

The solution of Eq. (31) is given by

$$|\psi(t)\rangle = e^{-iHt} |\psi(t=0)\rangle. \quad (35)$$

Therefore, the time evolution of Eqs. (26) and (27) can be computed by HS.

III. QSVT-BASED HAMILTONIAN SIMULATION

A. Oblivious amplitude amplification

Oblivious amplitude amplification (OAA) using QSVT has been proposed in Ref. [29]. In this section, we show the circuit of OAA and discuss the error and number of queries of the OAA-based HS. In the QSVT-based OAA, the d -th Chebyshev polynomial of the first kind, defined by $T_d(x) = \cos(d \arccos(x))$, is used as an objective function. For odd d , the corresponding phases $\Phi \in \mathbb{R}^{d+1}$ is given by

$$\begin{cases} \phi_0 = -\frac{d\pi}{2} \\ \phi_k = \frac{\pi}{2} \end{cases} \quad (k = 1, 2, \dots, d). \quad (36)$$

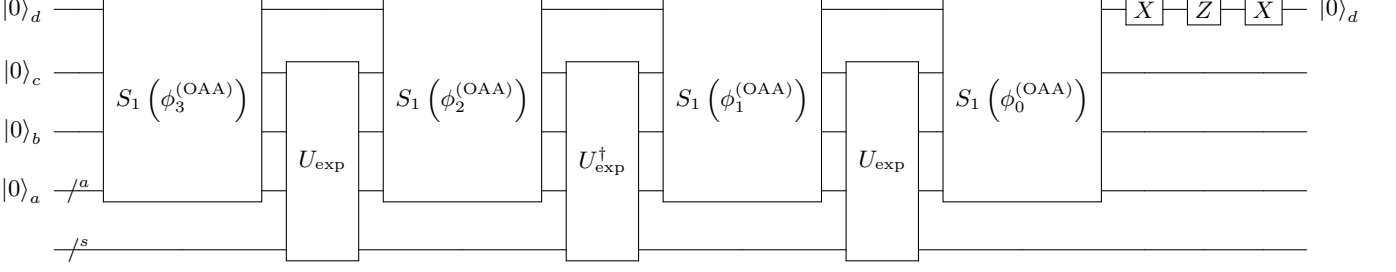


FIG. 3: Quantum circuit U_{OAA} that is a $(1, a + 2, \varepsilon)$ -block-encoding of $\exp(-iHt)$. The unitary U_{exp} is shown in Fig. 2, the gate S_1 is shown in Fig. 1(a), and the phases $\Phi^{(\text{OAA})} \in \mathbb{R}^4$ is given by Eq. (38).

Algorithm 1 The OAA-based Hamiltonian simulation

Input: a $(1, a, 0)$ -block-encoding of a Hamiltonian matrix H , an evolution time t , and an error tolerance ε .

Output: a $(1, a + 2, \varepsilon)$ -block-encoding of e^{-iHt}

Runtime: $Q_{\text{HS}}^{(\text{OAA})}$ queries to the block-encoding of H , where $Q_{\text{HS}}^{(\text{OAA})}$ is given by Eq. (41)

Procedure:

- 1: Calculate the phases $\Phi^{(c)} \in \mathbb{R}^{2R+1}$ and $\Phi^{(s)} \in \mathbb{R}^{2R+2}$ on a classical computer from the $2R$ -th polynomial $P_{\varepsilon_{\text{tri}}, \kappa}^{\text{cos}}(x)$ and $(2R + 1)$ -th polynomial $P_{\varepsilon_{\text{tri}}, \kappa}^{\text{sin}}(x)$ in Eq. (17), where $\kappa = 1/(1 + \varepsilon_{\text{tri}})$, $\varepsilon_{\text{tri}} = \varepsilon/9$ and R is given by Eq. (15).
 - 2: Construct the circuit U_{exp} in Fig. 2 using the phases $\Phi^{(c)}$ and $\Phi^{(s)}$, which is a $(1, a + 2, \kappa\varepsilon_{\text{tri}})$ -block-encoding of $\kappa e^{-iHt}/2$.
 - 3: Run the circuit U_{OAA} in Fig. 3 using the phases $\Phi^{(\text{OAA})} \in \mathbb{R}^4$ in Eq. (38).
-

From Eq. (18), the following inequality holds:

$$\begin{aligned}
& \left| \frac{e^{-ixt}}{2} - \frac{P_{\varepsilon_{\text{tri}}, \kappa}^{\text{cos}}(x) - iP_{\varepsilon_{\text{tri}}, \kappa}^{\text{sin}}(x)}{2} \right| \\
& \leq \left| \frac{\kappa\varepsilon_{\text{tri}}e^{-ixt}}{2} \right| + \left| \frac{\kappa e^{-ixt}}{2} - \frac{P_{\varepsilon_{\text{tri}}, \kappa}^{\text{cos}}(x) - iP_{\varepsilon_{\text{tri}}, \kappa}^{\text{sin}}(x)}{2} \right| \\
& \leq \frac{\kappa\varepsilon_{\text{tri}}}{2} + \kappa\varepsilon_{\text{tri}} \\
& = \frac{3\varepsilon_{\text{tri}}}{2(1 + \varepsilon_{\text{tri}})} < \frac{3}{2}\varepsilon_{\text{tri}}, \tag{37}
\end{aligned}$$

where in the first inequality we used the triangle inequality. Letting U be U_{exp} in Eq. (7) and using the following phases:

$$\begin{cases} \phi_0^{(\text{OAA})} = -\frac{3\pi}{2} \\ \phi_k^{(\text{OAA})} = \frac{\pi}{2} \end{cases} \quad (k = 1, 2, 3), \tag{38}$$

then one can get the block-encoding of

$$T_3\left(\frac{e^{-iHt}}{2}\right) = T_3\left(\cos\left(\frac{\pi}{3}\right)\right) e^{-iHt} = -e^{-iHt}, \tag{39}$$

where in the first equality we used that the singular value of a unitary matrix is 1. OAA multiplies the error by a factor of $2d$ [29]. Therefore, the quantum circuit U_{OAA} in Fig. 3 using the phases $\Phi^{(\text{OAA})}$ in Eq. (38) constructs the $(1, a + 2, 9\varepsilon_{\text{tri}})$ -block-encoding of $\exp(-iHt)$:

$$\|e^{-iHt} - (\langle 0|_{abc} \otimes I)U_{\text{OAA}}(|0\rangle_{abc} \otimes I)\| \leq 9\varepsilon_{\text{tri}}, \tag{40}$$

with 2 uses of U_{exp} and 1 use of U_{exp}^\dagger .

Given an error tolerance ε , the functions $\cos(xt)$ and $\sin(xt)$ should be $\frac{\varepsilon}{9}$ -approximated. Therefore, the number of queries of the OAA-based HS is given by

$$Q_{\text{HS}}^{(\text{OAA})} = 3\left(2R\left(t, \frac{\varepsilon}{9}\right) + 1\right) \leq \mathcal{O}(t + \log(1/\varepsilon)). \tag{41}$$

We summarize the OAA-based HS in Algorithm 1.

B. Fixed-point amplitude amplification

Fixed-point amplitude amplification (FPAA) using QSVT has been proposed in Refs. [29, 32]. In this section, the error and number of queries of the FPAA-based HS are investigated in detail. In QSVT-based FPAA, the sign function

$$\text{sign}(x) = \begin{cases} -1 & x < 0 \\ 0 & x = 0 \\ 1 & x > 0 \end{cases} \tag{42}$$

is chosen as an objective function. The sign function can be estimated by a polynomial approximation to an error function $\text{erf}(kx)$ for large enough k [32]. Let D be odd, $\Delta > 0$, and $\varepsilon_{\text{sign}} \in (0, \sqrt{2/e\pi})$. The phases $\Phi^{(\text{FPAA})} \in \mathbb{R}^{D+1}$ can be calculated from the D -th polynomial $P_{\varepsilon_{\text{sign}}, \Delta}^{\text{sign}}$ [29, 32] (the explicit form of $P_{\varepsilon_{\text{sign}}, \Delta}^{\text{sign}}$ is seen in Ref. [43]):

$$\begin{aligned}
& \left| \text{sign}(x) - P_{\varepsilon_{\text{sign}}, \Delta}^{\text{sign}}(x) \right| \leq \varepsilon_{\text{sign}} \\
& \text{for } x \in \left[-1, -\frac{\Delta}{2}\right] \cup \left[\frac{\Delta}{2}, 1\right]. \tag{43}
\end{aligned}$$

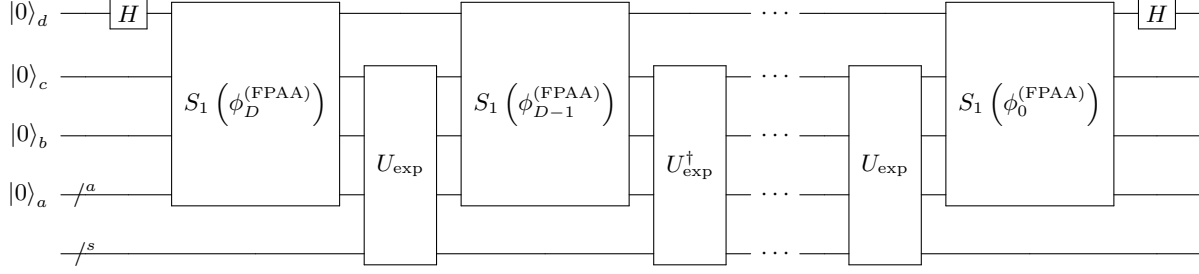


FIG. 4: Quantum circuit U_{FPAA} that is a $(1, a + 3, \varepsilon)$ -block-encoding of $\exp(-iHt)$. The unitary U_{exp} is shown in Fig. 2, the gate S_1 is shown in Fig. 1(a), and the phases $\Phi^{(\text{FPAA})} \in \mathbb{R}^{D+1}$ is calculated from the D -th polynomial $P_{\varepsilon_{\text{sign}}, \Delta}^{\text{sign}}$ that satisfies Eq. (43).

Algorithm 2 The FPAA-based Hamiltonian simulation

Input: a $(1, a, 0)$ -block-encoding of a Hamiltonian matrix H , an evolution time t , and an error tolerance ε .

Output: a $(1, a + 3, \varepsilon)$ -block-encoding of e^{-iHt}

Runtime: $Q_{\text{HS}}^{(\text{FPAA})}$ queries to the block-encoding of H , where $Q_{\text{HS}}^{(\text{FPAA})}$ is given by Eq. (53)

Procedure:

- 1: Calculate ε_{tri} and $\varepsilon_{\text{sign}}$ that minimize $Q_{\text{HS}}^{(\text{FPAA})}$, where R and D are given by Eqs. (15) and (44).
 - 2: Calculate the phases $\Phi^{(c)} \in \mathbb{R}^{2R+1}$ and $\Phi^{(s)} \in \mathbb{R}^{2R+2}$ on a classical computer from the $2R$ -th polynomial $P_{\varepsilon_{\text{tri}}, \kappa}^{\text{cos}}(x)$ and $(2R + 1)$ -th polynomial $P_{\varepsilon_{\text{tri}}, \kappa}^{\text{sin}}(x)$ in Eq. (17), where $\kappa = 1/(1 + \varepsilon_{\text{tri}})$.
 - 3: Construct the circuit U_{exp} in Fig. 2 using the phases $\Phi^{(c)}$ and $\Phi^{(s)}$, which is a $(1, a + 2, \kappa\varepsilon_{\text{tri}})$ -block-encoding of $\kappa e^{-iHt}/2$.
 - 4: Calculate the phases $\Phi^{(\text{FPAA})} \in \mathbb{R}^{D+1}$ on a classical computer from the D -th polynomial $P_{\varepsilon_{\text{sign}}, \kappa}^{\text{sign}}$ that satisfies Eq. (43).
 - 5: Run the circuit U_{FPAA} in Fig. 4 using the phases $\Phi^{(\text{FPAA})}$.
-

The degree D was given asymptotically in Ref. [29, 32]. We give it explicitly using the result of Ref. [43, 44]. If $k = \frac{\sqrt{2}}{\Delta} \log^{\frac{1}{2}}(8/[\pi\varepsilon_{\text{sign}}^2])$ and

$$D(k, \varepsilon_{\text{sign}}) = 2 \left\lceil \frac{16k}{\sqrt{\pi\varepsilon_{\text{sign}}}} \exp \left[-\frac{1}{2} W \left(\frac{512}{\pi\varepsilon_{\text{sign}}^2 e^2} \right) \right] \right\rceil + 1$$

$$= \mathcal{O} \left(\frac{1}{\Delta} \log(1/\varepsilon_{\text{sign}}) \right) \quad (44)$$

where W is the Lambert W function, then $P_{\varepsilon_{\text{sign}}, \Delta}^{\text{sign}}$ is $\varepsilon_{\text{sign}}$ -approximation to the sign function in the region $[-1, -\frac{\Delta}{2}] \cup [\frac{\Delta}{2}, 1]$. We require that $\Delta/2 \leq \kappa/2$ because we desire that $\kappa/2$ be mapped to a value greater than $1 - \varepsilon_{\text{sign}}$, and then $1/\Delta \geq 1/\kappa$. If $1/\Delta$ increases, then D increases because of $D \propto k \propto 1/\Delta$. Therefore, we should choose $\Delta = \kappa$.

We discuss the upper bound of the error of the FPAA-

based HS. Let us denote $A = \kappa \exp(-iHt)/2$ and $\tilde{A} = (\langle 0|_{abc} \otimes I) U_{\text{exp}}(|0\rangle_{abc} \otimes I)$. Equation (19) can be rewritten as

$$\|A - \tilde{A}\| \leq \kappa\varepsilon_{\text{tri}}, \quad (45)$$

and the following inequality holds:

$$\begin{aligned} \|A + \tilde{A}\| &\leq \|A\| + \|A\| + \|\tilde{A} - A\| \\ &\leq \frac{\kappa}{2} + \frac{\kappa}{2} + \kappa\varepsilon_{\text{tri}} \\ &= \kappa(1 + \varepsilon_{\text{tri}}) = 1, \end{aligned} \quad (46)$$

where in the first inequality we used the triangle inequality. Therefore, the matrices A and \tilde{A} satisfy the following inequality:

$$\begin{aligned} \|A - \tilde{A}\| + \left\| \frac{A + \tilde{A}}{2} \right\|^2 &\leq \kappa\varepsilon_{\text{tri}} + \frac{1}{4} \\ &= \frac{5}{4} - \frac{1}{1 + \varepsilon_{\text{tri}}} \\ &< \frac{5}{4} - \frac{e}{1 + e} < 1, \end{aligned} \quad (47)$$

where in the second last inequality we used $\varepsilon_{\text{tri}} < 1/e$. According to Lemma 23 in Ref. [29], we have that

$$\begin{aligned} &\left\| P_{\varepsilon_{\text{sign}}, \Delta}^{\text{sign}}(A) - P_{\varepsilon_{\text{sign}}, \Delta}^{\text{sign}}(\tilde{A}) \right\| \\ &\leq D \sqrt{\frac{2}{1 - \left\| \frac{A + \tilde{A}}{2} \right\|^2}} \|A - \tilde{A}\| \\ &\leq \sqrt{\frac{8}{3}} D \frac{\varepsilon_{\text{tri}}}{1 + \varepsilon_{\text{tri}}} < \sqrt{3} D \varepsilon_{\text{tri}}. \end{aligned} \quad (48)$$

Therefore, we have that

$$\begin{aligned} &\left\| \text{sign}(A) - P_{\varepsilon_{\text{sign}}, \Delta}^{\text{sign}}(\tilde{A}) \right\| \\ &\leq \left\| \text{sign}(A) - P_{\varepsilon_{\text{sign}}, \Delta}^{\text{sign}}(A) \right\| + \left\| P_{\varepsilon_{\text{sign}}, \Delta}^{\text{sign}}(A) - P_{\varepsilon_{\text{sign}}, \Delta}^{\text{sign}}(\tilde{A}) \right\| \\ &\leq \varepsilon_{\text{sign}} + \sqrt{3} D \varepsilon_{\text{tri}} \equiv \varepsilon'. \end{aligned} \quad (49)$$

TABLE I: The comparison between OAA-based and FPAA-based HS.

	OAA-based HS	FPAA-based HS
Polynomial used	$T_3(x)$	The approximate polynomial of $\text{sign}(x)$
The number of queries	$3(2R(t, \frac{\varepsilon}{9}) + 1)$	$D(\kappa, \varepsilon_{\text{sign}})(2R(t, \varepsilon_{\text{tri}}) + 1)$
Asymptotic query complexity	$\mathcal{O}(t + \log(1/\varepsilon))$	$\mathcal{O}(\log(1/\varepsilon)t + \log^2(1/\varepsilon))$

From the above inequality, we have that $\|P_{\varepsilon_{\text{sign}}, \Delta}^{\text{sign}}(\tilde{A})\| \leq 1 + \varepsilon'$, which violates the condition (vi). Therefore, we must consider the rescaled polynomial $\frac{1}{1+\varepsilon'} P_{\varepsilon_{\text{sign}}, \Delta}^{\text{sign}}(\tilde{A})$ such that $\frac{1}{1+\varepsilon'} \|P_{\varepsilon_{\text{sign}}, \Delta}^{\text{sign}}(\tilde{A})\| \leq 1$. Now, we obtain the following inequality:

$$\begin{aligned} & \left\| \text{sign}(A) - \frac{1}{1+\varepsilon'} P_{\varepsilon_{\text{sign}}, \Delta}^{\text{sign}}(\tilde{A}) \right\| \\ & \leq \frac{1}{1+\varepsilon'} \left(\|\text{sign}(A) - P_{\varepsilon_{\text{sign}}, \Delta}^{\text{sign}}(\tilde{A})\| + \|\varepsilon' \text{sign}(A)\| \right) \\ & \leq \frac{\varepsilon' + \varepsilon'}{1+\varepsilon'} < 2\varepsilon', \end{aligned} \quad (50)$$

and the error tolerance is defined as

$$\varepsilon \equiv 2\varepsilon' = 2 \left(\varepsilon_{\text{sign}} + \sqrt{3}D\varepsilon_{\text{tri}} \right). \quad (51)$$

The quantum circuit U_{FPAA} using the phases $\Phi^{(\text{FPAA})} \in \mathbb{R}^{D+1}$ in Fig. 4 constructs the $(1, a+3, \varepsilon)$ -block-encoding of $\exp(-iHt)$:

$$\|e^{-iHt} - (\langle 0|_{abcd} \otimes I)U_{\text{FPAA}}(|0\rangle_{abcd} \otimes I)\| \leq \varepsilon, \quad (52)$$

with $(D+1)/2$ uses of U_{exp} and $(D-1)/2$ uses of U_{exp}^\dagger . Therefore, the number of queries of the FPAA-based HS is given by $D(2R+1)$. It varies depending on ε_{tri} and $\varepsilon_{\text{sign}}$ satisfying Eq. (51). The number of queries of the FPAA-based HS is defined as

$$Q_{\text{HS}}^{(\text{FPAA})} = \min_{\varepsilon_{\text{tri}}, \varepsilon_{\text{sign}}} D(\kappa, \varepsilon_{\text{sign}})(2R(t, \varepsilon_{\text{tri}}) + 1). \quad (53)$$

This is asymptotically given by

$$\begin{aligned} Q_{\text{HS}}^{(\text{FPAA})} &= \mathcal{O}(\log(1/\varepsilon_{\text{sign}})[t + \log(1/\varepsilon_{\text{tri}})]) \\ &= \mathcal{O}(\log(1/\varepsilon)t + \log^2(1/\varepsilon)). \end{aligned} \quad (54)$$

We summarize the FPAA-based HS in Algorithm 2; also we summarize the comparison between OAA-based and FPAA-based HS in Table I.

C. Hamiltonian simulation for general Hermitian matrix and extension of evolution time

We describe the way to implement HS for a general Hermitian matrix H that is not positive semidefinite and

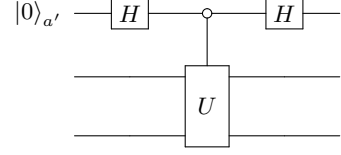


FIG. 5: Construction of the unitary U' that is a $(1, a+1, 0)$ -block-encoding of $(H/\alpha + I)/2$ from the unitary U , defined as in Eq. (55).

normalized by $\alpha > 0$, i.e., $\|H/\alpha\| \leq 1$. Suppose that U is an $(\alpha, a, 0)$ -block-encoding of H :

$$U = \begin{bmatrix} \frac{H}{\alpha} & \cdot \\ \cdot & \cdot \end{bmatrix}, \quad \frac{H}{\alpha} = (\langle 0|_a \otimes I)U(|0\rangle_a \otimes I). \quad (55)$$

The authors of Ref. [32] have proposed the unitary U' as in Fig. 5, which is a $(1, a+1, 0)$ -block-encoding of the positive semidefinite Hermitian matrix $(H/\alpha + I)/2$. Instead of U , this unitary is used in the circuits U_{exp} , and U_{OAA} or U_{FPAA} , denoted by U_{HS} . Then, U_{HS} becomes a $(1, a+3, \varepsilon)$ -block-encoding of $\exp(-i\frac{H/\alpha+I}{2}t)$:

$$\left\| e^{-i\frac{H/\alpha+I}{2}t} - (\langle 0|_{aa'bc} \otimes I)U_{\text{HS}}(|0\rangle_{aa'bc} \otimes I) \right\| \leq \varepsilon. \quad (56)$$

If the evolution time t is modified to $2\alpha t$, then U_{HS} becomes a $(1, a+3, \varepsilon)$ -block-encoding of e^{-iHt} up to a global phase. Therefore, the query complexity of QSVT-based HS can be generally represented as

$$\mathcal{O}(2\alpha t + \log(1/\varepsilon)). \quad (57)$$

Note that the factor $\log(1/\varepsilon)$ is multiplied by the above complexity for the FPAA-based HS, but it is ignored for simplicity.

Larger t requires calculating a higher number of the phases, which can be challenging. One can instead use N_t sequential U_{HS} for the smaller time step $\Delta t = t/N_t$ and extend the evolution time as follows:

$$e^{-iHt} \approx (\langle 0|_{aa'bc} \otimes I)U_{\text{HS}}^{N_t}(\langle 0|_{aa'bc} \otimes I). \quad (58)$$

This split is also found in Ref. [11]. We discuss the query complexity of the extension of the evolution time of HS. According to Lemma 53 in Ref. [29], the error of the product of two block-encoded matrices does not exceed the sum of each error. Let U_{HS} be a $(1, a+3, \delta)$ -block-encoding of $\exp(-iH\Delta t)$, and then we have that

$$\left\| e^{-iHt} - (\langle 0|_{aa'bc} \otimes I)U_{\text{HS}}^{N_t}(|0\rangle_{aa'bc} \otimes I) \right\| \leq N_t\delta \equiv \varepsilon, \quad (59)$$

where ε is an error tolerance. The query complexity in Eq. (57) can be rewritten as follows:

$$\begin{aligned} & N_t \mathcal{O} \left(2\alpha\Delta t + \log \left(\frac{1}{\delta} \right) \right) \\ &= \mathcal{O} \left(2\alpha t + N_t \log \left(\frac{N_t}{\varepsilon} \right) \right). \end{aligned} \quad (60)$$

IV. QUANTUM ALGORITHM FOR THE LINEARIZED VLASOV-POISSON SYSTEM

Quantum algorithms for the linearized Vlasov-Poisson system have three steps: (1) initialization, (2) HS, and (3) Extracting data. Initialization prepares a quantum state that represents initial physical conditions; HS implements the time evolution of Eq. (31); Extracting physically meaningful data from a final state.

To encode data and construct the Hamiltonian H , we use a rotation gate called a variable rotation introduced in Ref. [9], defined as

$$R(x) \equiv \begin{cases} e^{-iY \arccos x} & (x \in \mathbb{R}) \\ e^{-iX \arccos \text{Im}(x)} e^{iZ \frac{\pi}{2}} & (x \in \mathbb{C} \setminus \mathbb{R}), \end{cases} \quad (61)$$

where x is a rotation angle such that $|x| \leq 1$. This gate acts as $R(x)|0\rangle = x|0\rangle + \sqrt{1-|x|^2}|1\rangle$. We assume that the rotation angles can be calculated efficiently on temporary registers, and applying the rotations controlled on the angle qubits can be implemented efficiently. Then the cost to implement the variable rotations is $\mathcal{O}(\text{poly}(n_v)) = \mathcal{O}(\text{poly}(\log N_v))$ because the input register has n_v qubits.

A. The one-dimensional linearized Vlasov-Poisson system

Efficiently preparing a quantum state that represents the physical data is a very difficult problem. This problem is related to amplitude encoding [45]. Assuming quantum random access memory (QRAM) [46], amplitude encoding is also implemented efficiently. Under this assumption, we desire that a quantum circuit for initialization $U_{\text{ini}}^{\text{ideal}}$ can prepare the following initial state:

$$U_{\text{ini}}^{\text{ideal}} |0\rangle_r |0\rangle_v = \frac{1}{\eta} \left[\sum_{j_x=0}^{N_{v_x}-1} F_{j_x}(t=0) |0\rangle_r |j_x\rangle_{v_x} + E(t=0) |1\rangle_r |0\rangle_{v_x} \right], \quad (62)$$

where $\eta = \sqrt{\sum_{j_x} |F_{j_x}(t=0)|^2 + |E(t=0)|^2}$. We assume the gate complexity of $U_{\text{ini}}^{\text{ideal}}$ is $\mathcal{O}(\text{poly}(\log N_{v_x}))$.

To implement HS for the linearized Vlasov-Poisson system, it is necessary to construct the corresponding unitary U that is an $(\alpha, a, 0)$ -block-encoding of H . The unitary for the one-dimensional system has been proposed in Ref. [9], which consists of two unitaries U_{row} and U_{col} . These unitaries are called state preparation unitaries in Ref. [29] and satisfy $U = U_{\text{row}}^\dagger U_{\text{col}}$. The gate complexity of U is given by $\mathcal{O}(\text{poly}(\log N_{v_x}))$. According to Ref. [9], α satisfies the following inequality:

$$\frac{4\Lambda}{5} \leq \alpha \leq \Lambda, \quad (63)$$

where

$$\begin{aligned} \Lambda &= |k_x| v_{x,\text{max}} + \sqrt{\Delta v_x N_{v_x} v_{x,\text{max}} G_{\text{max}}}, \\ v_{x,\text{max}} &= \max_{j_x} |v_{j_x}|, \\ G_{\text{max}} &= \max_{j_x} |v_{j_x} f_M(v_{v_{j_x}})|. \end{aligned} \quad (64)$$

Since $\Delta v_x N_{v_x} = 2v_{x,\text{max}} + \Delta v_x$, Λ does not increase with increasing N_{v_x} , i.e. $\alpha = \Theta(1)$. Therefore, the query complexity of QSVT-based HS is given by $\mathcal{O}(t + \log(1/\varepsilon))$. The gate complexity of QSVT-based HS is the above equation multiplied by $\text{poly}(\log N_{v_x})$.

One of the ways to obtain data from the final state is the quantum amplitude estimation (QAE) algorithm [38], which can produce an estimate \tilde{p} of the probability p with an error bounded by

$$|\tilde{p} - p| \leq 2\pi \frac{\sqrt{p(1-p)}}{M} + \frac{\pi^2}{M^2}, \quad (65)$$

where M is the number of iterations. The authors of Ref. [9] have used QAE to obtain an estimate of the magnitude $|E|$. They have also proposed the algorithm for obtaining the real and imaginary parts of E and showed its cost does not change asymptotically. We discuss the computational complexity of calculating the time evolution of E , and the algorithm for obtaining quantities related to the distribution function f .

The state after HS for the evolution time t is applied to the initial state in Eq. (62) becomes

$$|\psi(t)\rangle = \frac{1}{\eta} |0\rangle_a \left[\sum_{j_x=0}^{N_{v_x}-1} F_{j_x}(t) |0\rangle_r |j_x\rangle_{v_x} + E(t) |1\rangle_r |0\rangle_{v_x} \right], \quad (66)$$

where label a is represented as all ancilla qubits including qubits labeled a, a', b, c , and d . Let $p = |E(t)|^2/\eta^2$ and its estimate be \tilde{p} . We introduce $a = |E(t)|^2$ and $\tilde{a} = \eta^2 \tilde{p}$ and then they satisfy the following inequality from Eq. (65):

$$\begin{aligned} |\tilde{a} - a| &\leq 2\pi \frac{\sqrt{a(\eta^2 - a)}}{M} + \frac{\pi^2 \eta^2}{M^2} \\ &\leq \frac{2\pi \eta |E(t)|}{M} + \frac{\pi^2 \eta^2}{M^2}, \end{aligned} \quad (67)$$

where in the last inequality we used $\eta^2 - a \leq \eta^2$. Assuming we know the upper bound of $|E(t)|$ is E_u . Let $0 < \delta < 1$ and $M = \left\lceil \frac{(2E_u+1)\pi\eta}{\delta} \right\rceil$. The above inequality becomes

$$\begin{aligned} |\tilde{a} - a| &\leq \frac{2|E(t)|\delta}{2E_u+1} + \frac{\delta^2}{(2E_u+1)^2} \\ &\leq \frac{2|E(t)|\delta}{2E_u+1} + \frac{\delta}{2E_u+1} \leq \delta, \end{aligned} \quad (68)$$

where in the last inequality we used $2|E(t)|+1 \leq 2E_u+1$. The value of $E(t)$ can also be obtained asymptotically with the same complexity at an additional cost using the algorithm proposed in Ref. [9].

Since $M = \mathcal{O}(1/\delta)$, the gate complexity of the whole algorithm for obtaining the estimate of $E(t)$ including the initialization and HS steps is given by:

$$\mathcal{O}\left(\frac{\text{poly}(\log N_v)}{\delta}(t + \log(1/\varepsilon))\right). \quad (69)$$

Now, we discuss the cost of calculating the time evolution of E . For simplicity, we assume the phases $\Phi^{(c)}$ and $\Phi^{(s)}$ for a large t , and given error tolerance ε can be calculated. Let N_t be the number of time steps, t_{\max} be the maximum of the evolution time, and $\Delta t = t_{\max}/N_t$ be the time step. The gate complexity of the algorithm for the evolution time $t_l = l\Delta t$ is given by Eq. (69) with t replaced by t_l , denoted by Q_l . Since

$$\sum_{l=1}^{N_t} t_l = \frac{\Delta t}{2} N_t(N_t + 1) = \frac{t_{\max}(N_t + 1)}{2}, \quad (70)$$

the gate complexity of calculating the time evolution of E is

$$\sum_{l=1}^{N_t} Q_l = \mathcal{O}\left(\frac{\text{poly}(\log N_v)N_t}{\delta}(t_{\max} + \log(1/\varepsilon))\right). \quad (71)$$

If we consider t_{\max} to be a constant, then the cost of the quantum algorithm is asymptotically the same for the number of time steps N_t as that of a classical algorithm, which scales linearly with N_t .

We show the way to obtain the deviation from the Maxwell distribution

$$\begin{aligned} D_M(t) &\equiv \sum_{j_x=0}^{N_{v_x}-1} |f(v_{j_x}, t) - f_M(v_{j_x})|^2 \Delta v_x \\ &= \sum_{j_x=0}^{N_{v_x}-1} |f_1(v_{j_x}, t)|^2 \Delta v_x. \end{aligned} \quad (72)$$

Here, we write the subscript 1 explicitly. This quantity can be used to know how well the fluid approximation is applied to the system. We add single ancilla qubit and variable rotation gates with angles $\sqrt{f_M(v_{j_x})}$, and the state in Eq. (66) becomes as follows:

$$\frac{1}{\eta} \sum_{j_x=0}^{N_{v_x}-1} i f_1(v_{j_x}, t) \sqrt{\Delta v_x} |0\rangle_\alpha |0\rangle_r |j_x\rangle_{v_x} |0\rangle + |\perp\rangle, \quad (73)$$

where $|\perp\rangle$ is the state of no interest. QAE is applied to the above state, we obtain the estimate

$$\tilde{p} \approx \frac{1}{\eta^2} \sum_{j_x=0}^{N_{v_x}-1} |f_1(v_{j_x}, t)|^2 \Delta v_x = \frac{1}{\eta^2} D_M(t). \quad (74)$$

Similar to the discussion of QAE to obtain the estimate of $E(t)$, the number of iterations to obtain the estimate of D_M is also given by $M = \mathcal{O}(1/\delta)$. Therefore, the gate complexity of the algorithm for calculating the deviation D_M is given by Eq. (69).

B. The higher dimensional Vlasov-Poisson systems

The discussion of initialization and extracting data steps for the one-dimensional linearized Vlasov-Poisson system can easily be extended to the higher system. In this section, we focus on the construction of unitaries $U = U_{\text{row}}^\dagger U_{\text{col}}$ that are $(\alpha, a, 0)$ -block-encoding of H for the higher systems.

We show the circuits U_{row} and U_{col} for the two-dimensional system in Figs. 6 and 7. The unitary U is an $(\alpha, 6, 0)$ -block-encoding of the Hamiltonian H :

$$\begin{aligned} \frac{H}{\alpha} &= \sum_j \left[c^2 b_j^2 |0\rangle_r |j\rangle_v \langle 0|_r \langle j|_v \right. \\ &+ \frac{\sqrt{1-|c|^2} d_j}{\sqrt{2N_v}} \left(p_{j_x} (|0\rangle_r |j\rangle_v \langle 1|_r \langle \mathbf{0}|_v + |1\rangle_r |0\rangle_v \langle 0|_r \langle j|_v) \right. \\ &\left. \left. + q_{j_y} (|0\rangle_r |j\rangle_v \langle 2|_r \langle \mathbf{0}|_v + |2\rangle_r |0\rangle_v \langle 0|_r \langle j|_v) \right) \right] + \hat{D}_2, \end{aligned} \quad (75)$$

where \hat{D}_2 is the unused subspace. Comparing Eq. (34) for the two-dimensional system with Eq. (75), we obtain

$$\begin{aligned} c^2 b_j^2 &= \frac{k_x v_{j_x} + k_y v_{j_y}}{\alpha}, \\ \sqrt{1-|c|^2} \frac{p_{j_x} d_j}{\sqrt{2N_v}} &= \frac{\mu_j v_{j_x}}{\alpha}, \\ \sqrt{1-|c|^2} \frac{q_{j_y} d_j}{\sqrt{2N_v}} &= \frac{\mu_j v_{j_y}}{\alpha}, \end{aligned} \quad (76)$$

where $N_v = N_{v_x} N_{v_y}$. The angles $b_j, d_j, p_{j_x}, q_{j_y}$ are chosen as follows:

$$\begin{aligned} b_j &= \sqrt{\frac{k_x v_{j_x} + k_y v_{j_y}}{K_{\max}}}, \quad d_j = \sqrt{\frac{f_M(v_j)}{g_{\max}}}, \\ p_{j_x} &= \frac{v_{j_x}}{V_{\max}}, \quad q_{j_y} = \frac{v_{j_y}}{V_{\max}}, \end{aligned} \quad (77)$$

where

$$\begin{aligned} K_{\max} &= \max_j |k_x v_{j_x} + k_y v_{j_y}|, \\ g_{\max} &= \max_j f_M(v_{j_x}, v_{j_y}), \\ V_{\max} &= \max_{j_x} |v_{j_x}| \max_{j_y} |v_{j_y}| = v_{x,\max} v_{y,\max}. \end{aligned} \quad (78)$$

Note that we assume $v_{x,\max} \geq 1, v_{y,\max} \geq 1$ to make $|p_{j_x}| \leq 1, |q_{j_y}| \leq 1$ hold. From Eqs. (76) and (77), c and α are given by

$$c^2 = \frac{\Gamma}{2} \left(\sqrt{1 + \frac{4}{\Gamma}} - 1 \right), \quad (79)$$

$$\alpha = \frac{K_{\max}}{c^2}, \quad (80)$$

where

$$\Gamma = \frac{K_{\max}^2}{2\Delta v N_v V_{\max}^2 g_{\max}}, \quad (81)$$

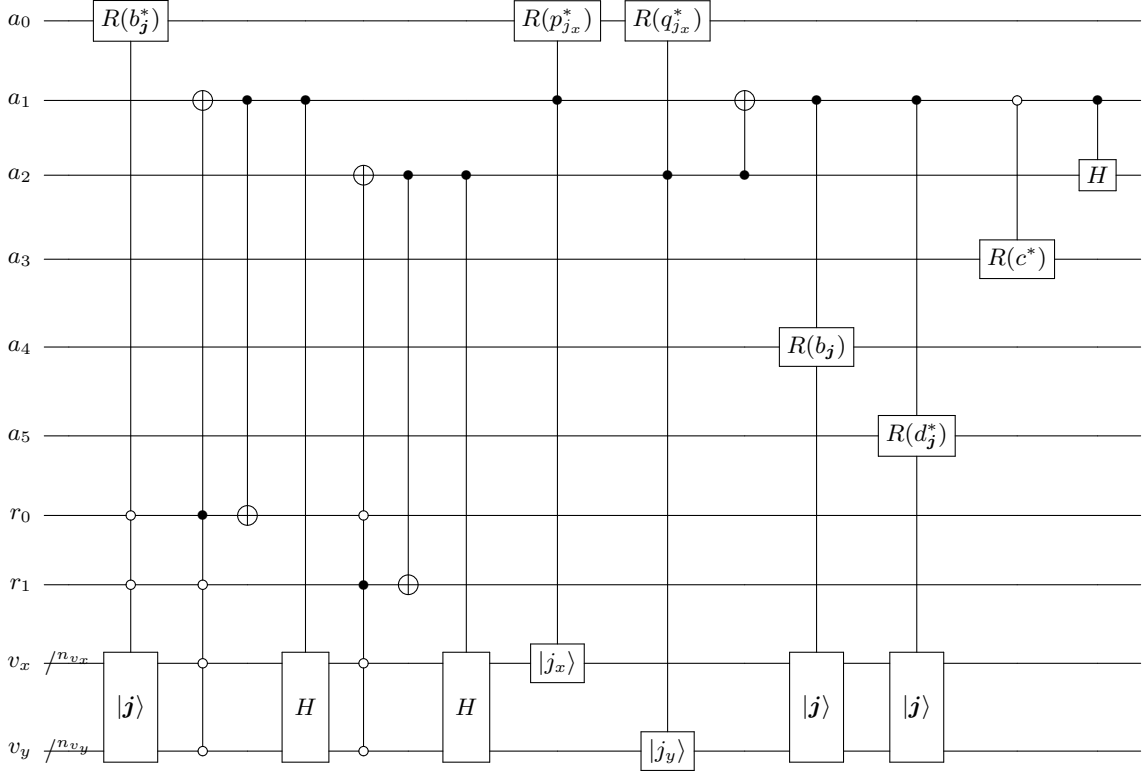


FIG. 6: Quantum circuit of the unitary U_{row} for the two-dimensional linearized Vlasov-Poisson system.

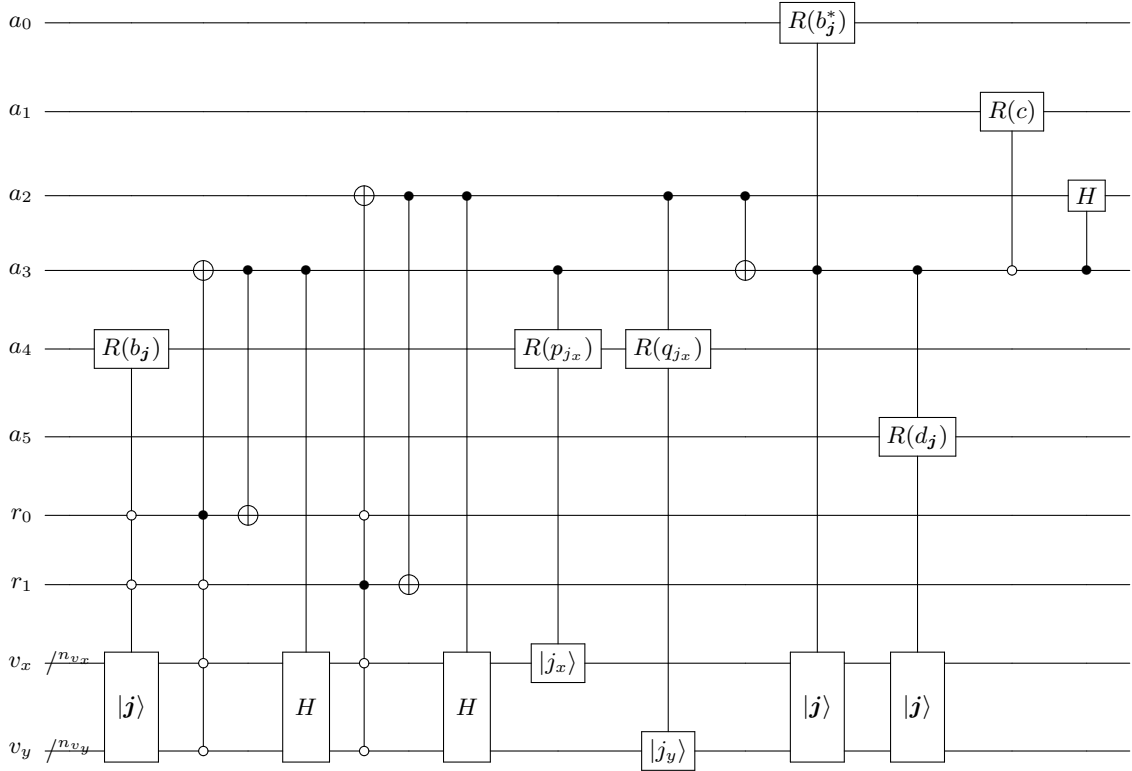


FIG. 7: Quantum circuit of the unitary U_{col} for the two-dimensional linearized Vlasov-Poisson system.

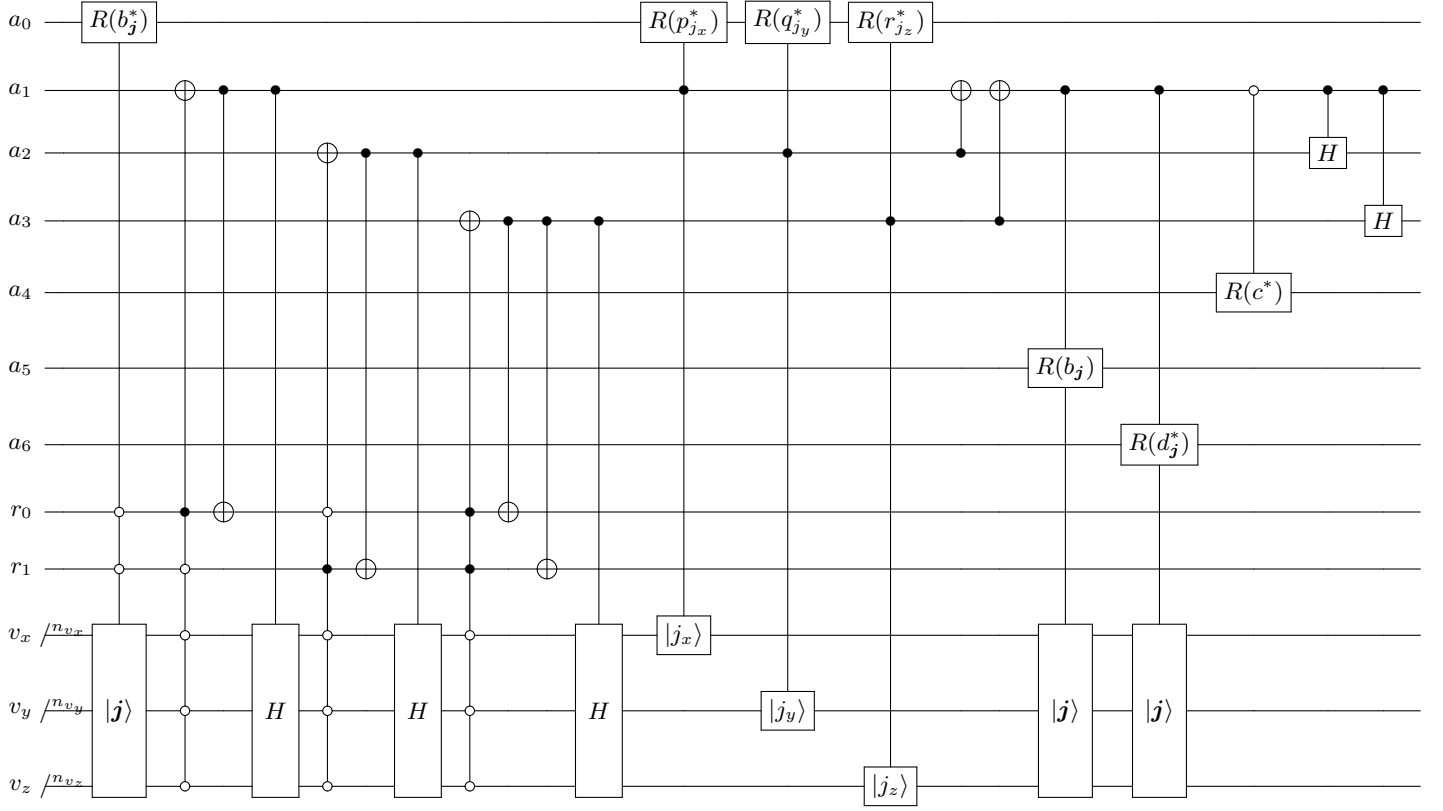


FIG. 8: Quantum circuit of the unitary U_{row} for the three-dimensional linearized Vlasov-Poisson system.

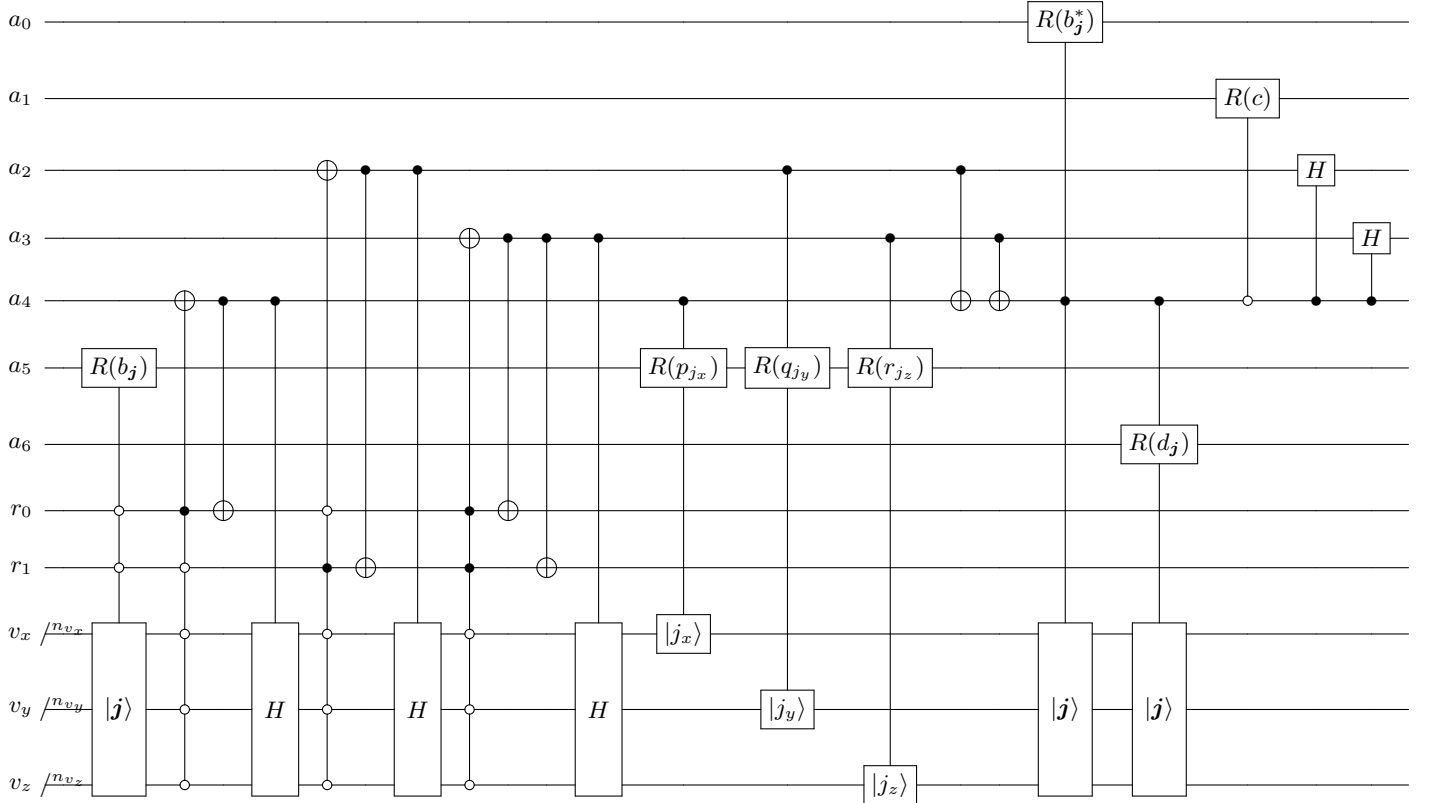


FIG. 9: Quantum circuit of the unitary U_{col} for the three-dimensional linearized Vlasov-Poisson system.

TABLE II: Comparison of Hamiltonian simulation for the linearized Vlasov-Poisson system. The system register is defined as register labeled by r and v .

Dimension	The total grid size N_v	The number of system register	The number of ancilla qubits of U	Gate complexity
1	N_{v_x}	$n_{v_x} + 1$	4	
2	$N_{v_x} N_{v_y}$	$n_{v_x} + n_{v_y} + 2$	6	$\mathcal{O}(\text{poly}(\log N_v)(t + \log(1/\varepsilon)))$
3	$N_{v_x} N_{v_y} N_{v_z}$	$n_{v_x} + n_{v_y} + n_{v_z} + 2$	7	

and $\Delta v = \Delta v_x \Delta v_y$. As for the one-dimensional system, α satisfies the following inequality:

$$\frac{4\Lambda}{5} \leq \alpha \leq \Lambda, \quad (82)$$

where

$$\Lambda = K_{\max} + \sqrt{2\Delta v N_v V_{\max}^2 g_{\max}}. \quad (83)$$

Since $\Delta v N_v = (2v_{x,\max} + \Delta v_x)(2v_{y,\max} + \Delta v_y)$, if N_v increases, then Λ does not increase, i.e. $\alpha = \Theta(1)$. Therefore, the query complexity also does not increase with increasing N_v . In addition, the gate complexity scales logarithmically with N_v because the input register of the variable rotations in Fig. 6 and 7 has $n_{v_x} + n_{v_y}$ qubits. These results are the same as for the one-dimensional system.

We show a unitary $U = U_{\text{row}}^\dagger U_{\text{col}}$ for the three-dimensional Vlasov-Poisson system and similar results to the ones for the lower dimensional systems. The circuits U_{row} and U_{col} are shown in Figs. 8 and 9. The unitary U is an $(\alpha, 7, 0)$ -block-encoding of the Hamiltonian H :

$$\begin{aligned} \frac{H}{\alpha} = & \sum_j \left[c^2 b_j^2 |0\rangle_r |j\rangle_v \langle 0|_r \langle j|_v \right. \\ & + \frac{\sqrt{1-|c|^2} d_j}{2\sqrt{N_v}} \left(p_{j_x} (|0\rangle_r |j\rangle_v \langle 1|_r \langle \mathbf{0}|_v + |1\rangle_r |0\rangle_v \langle 0|_r \langle j|_v) \right. \\ & + q_{j_y} (|0\rangle_r |j\rangle_v \langle 2|_r \langle \mathbf{0}|_v + |2\rangle_r |0\rangle_v \langle 0|_r \langle j|_v) \\ & \left. \left. + r_{j_z} (|0\rangle_r |j\rangle_v \langle 3|_r \langle \mathbf{0}|_v + |3\rangle_r |0\rangle_v \langle 0|_r \langle j|_v) \right) \right] + \hat{D}_3, \end{aligned} \quad (84)$$

where $N_v = N_{v_x} N_{v_y} N_{v_z}$ and \hat{D}_3 is the unused subspace. The corresponding angles and α are as follows:

$$\begin{aligned} b_j &= \sqrt{\frac{k_x v_{j_x} + k_y v_{j_y} + k_z v_{j_z}}{K_{\max}}}, \\ d_j &= \sqrt{\frac{f_M(v_j)}{g_{\max}}}, \quad p_{j_x} = \frac{v_{j_x}}{V_{\max}}, \\ q_{j_y} &= \frac{v_{j_y}}{V_{\max}}, \quad r_{j_z} = \frac{v_{j_z}}{V_{\max}}, \end{aligned} \quad (85)$$

$$c^2 = \frac{\Gamma}{2} \left(\sqrt{1 + \frac{4}{\Gamma}} - 1 \right), \quad (86)$$

$$\alpha = \frac{K_{\max}}{c^2}, \quad (87)$$

where

$$\begin{aligned} K_{\max} &= \max_j |k_x v_{j_x} + k_y v_{j_y} + k_z v_{j_z}|, \\ g_{\max} &= \max_j f_M(v_{j_x}, v_{j_y}, v_{j_z}), \\ V_{\max} &= v_{x,\max} v_{y,\max} v_{z,\max}, \\ \Gamma &= \frac{K_{\max}^2}{4\Delta v N_v V_{\max}^2 g_{\max}}. \end{aligned} \quad (88)$$

As for the lower dimensional system, α satisfies the following inequality:

$$\frac{4\Lambda}{5} \leq \alpha \leq \Lambda, \quad (89)$$

where

$$\Lambda = K_{\max} + \sqrt{4\Delta v N_v V_{\max}^2 g_{\max}}. \quad (90)$$

Since $\Delta v N_v = (2v_{x,\max} + \Delta v_x)(2v_{y,\max} + \Delta v_y)(2v_{z,\max} + \Delta v_z)$, if N_v increases, then Λ does not increase. Therefore, the same result is obtained for the query complexity and the gate complexity. We summarize the computational resources of HS for the linearized Vlasov-Poisson system in Table II.

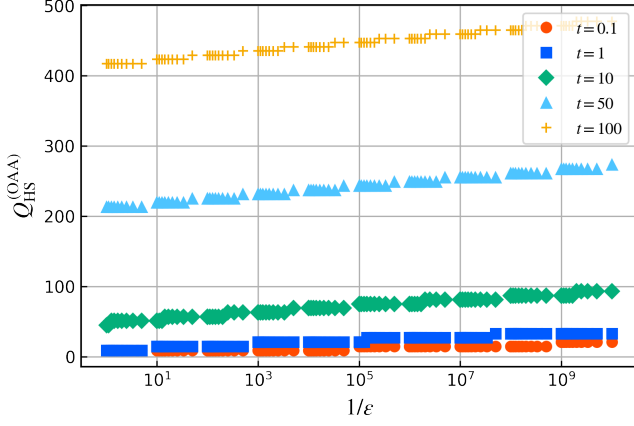
V. NUMERICAL RESULTS

A. QSVT-based Hamiltonian simulation

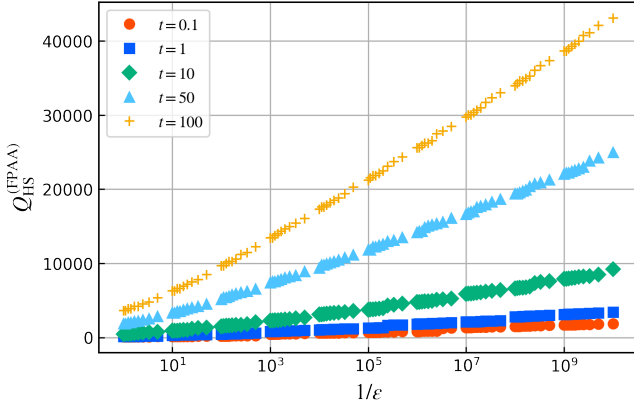
We compare the number of queries of the OAA-based and FPAA-based HS algorithms. The number of queries for some given error tolerances ε and evolution times t calculated from Eqs. (41) and (53) is shown in Figs. 10 and 11. Notably, the number of queries of the OAA-based HS is significantly smaller than that of the FPAA-based one for all parameters. These figures show that the number of queries $Q_{\text{HS}}^{(\text{OAA})}$ and $Q_{\text{HS}}^{(\text{FPAA})}$ scale linearly for t and linearly and quadratically for $\log(1/\varepsilon)$, respectively. These results are consistent with the asymptotic scaling of Eqs. (41) and (54).

To identify the constant factors and coefficients of the number of queries hidden behind the asymptotic scaling, we fit the curve for OAA with

$$Q_{\text{HS}}^{(\text{OAA})} = \alpha_0 + \alpha_1 t + \alpha_2 \log(1/\varepsilon), \quad (91)$$



(a) OAA-based HS.



(b) FPAA-based HS.

FIG. 10: The number of queries vs. $1/\epsilon$.

TABLE III: The constant factors and coefficients of Eqs. (41), (53).

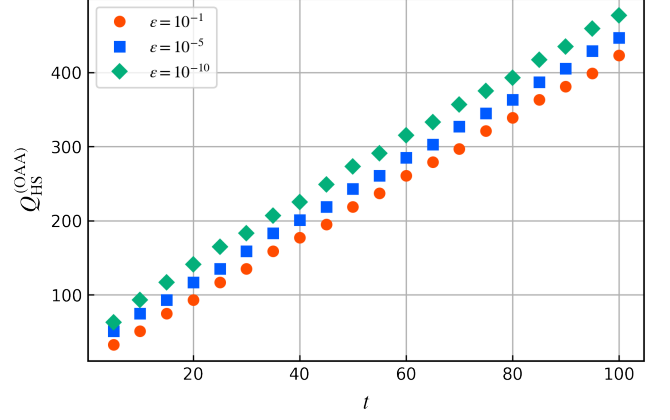
Method	Range of parameters	α_0	α_1	α_2	α_3	α_4
OAA	$0.1 \leq t \leq 10$ $10^{-5} \leq \epsilon \leq 0.9$	2.73	4.88	1.78		
OAA	$1 \leq t \leq 100$ $10^{-10} \leq \epsilon \leq 0.9$	2.77	4.18	2.45		
FPAA	$0.1 \leq t \leq 10$ $10^{-5} \leq \epsilon \leq 0.9$	142	28.3	11.9	20.9	7.26
FPAA	$1 \leq t \leq 100$ $10^{-10} \leq \epsilon \leq 0.9$	490	21.7	-15.6	15.4	10.9

and the curve for FPAA with

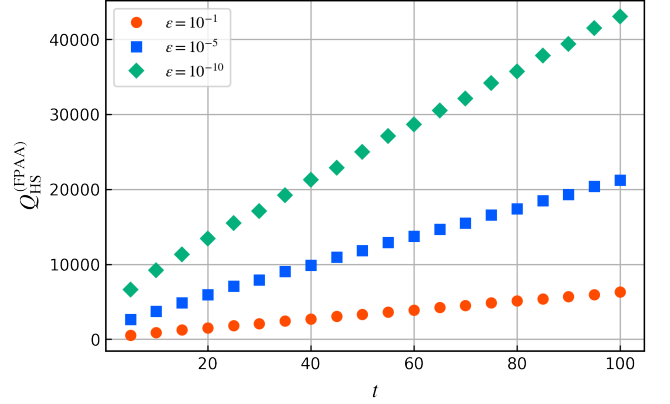
$$Q_{\text{HS}}^{(\text{FPAA})} = \alpha_0 + \alpha_1 t + \alpha_2 \log(1/\epsilon) + \alpha_3 t \log(1/\epsilon) + \alpha_4 \log^2(1/\epsilon). \quad (92)$$

The results are presented in Table III. Both values of FPAA are greater than those of OAA. Thus, OAA proves more effective for HS than FPAA in terms of the number of queries.

We emphasize that the advantage of OAA over FPAA in HS is a general result. The reasons for this can be



(a) OAA-based HS.



(b) FPAA-based HS.

FIG. 11: The number of queries vs. t .

explained as follows. The number of queries is calculated from Eqs. (41) and (53). These equations are derived under the general assumption that the Hamiltonian is positive semidefinite and its norm is less than 1; that is, Eqs. (41) and (53) hold without respect to the type of the Hamiltonian. Therefore, from the theoretical and numerical results of the number of queries, OAA is more advantageous than FPAA in Hamiltonian simulations of general systems.

To specify which degree of approximation of trigonometric functions or sign function dominates the number of queries of FPAA-based HS, we fit the curves for R and D in Eq. (53) with

$$R = \alpha_0 + \alpha_1 t + \alpha_2 \log(1/\epsilon), \quad (93)$$

$$D = \alpha_0 + \alpha_2 \log(1/\epsilon), \quad (94)$$

for $0.1 \leq t \leq 10, 10^{-5} \leq \epsilon \leq 0.9$. Then we obtain the following results: for R ,

$$\alpha_0 = 0.853, \quad \alpha_1 = 0.913, \quad \alpha_2 = 0.293, \quad (95)$$

for D ,

$$\alpha_0 = 21.8, \quad \alpha_2 = 10.1. \quad (96)$$

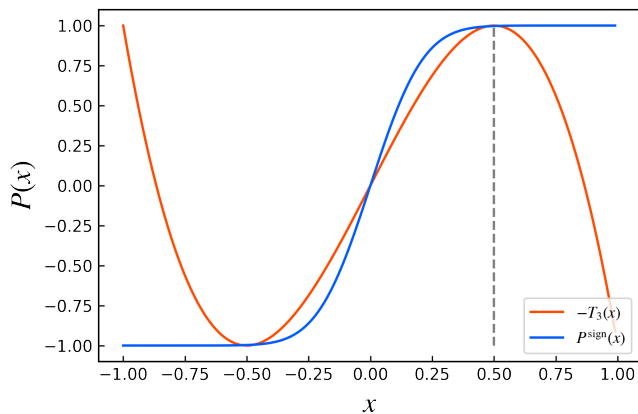


FIG. 12: Illustration of the difference between amplitude amplifications in OAA-based and FPAA-based HS.

The constant factors and coefficients of D are larger than those of R . Thus, the large number of queries of FPAA-based HS is caused by requiring a high degree of approximation of the sign function.

We now explain the intuitive reason why it is not appropriate to use a sign function for amplitude amplification in QSVT-based HS. As seen in Sec. II B, the specific amplitude value $\kappa/2 \approx 1/2$ must be amplified in QSVT-based HS. For OAA-based HS, the 3rd Chebyshev polynomial is precisely $|T_3(x)| = 1$ at $x = 1/2$, whereas for the FPAA-based one, the sign function is $\text{sign}(x) = 1$ for $1/2 \leq x \leq 1$. The OAA-based method amplifies the value exclusively at $x = 1/2$. In contrast, the FPAA-based method aims to amplify the values for $1/2 \leq x \leq 1$, leading to extra, unneeded effort for amplification in this range, as depicted in Fig. 12. This results in a high degree of approximation of the sign function and many queries for FPAA-based HS.

B. Application to the linearized Vlasov-Poisson system

Here, the OAA-based HS is applied to the simulation of the one-dimensional linearized Vlasov-Poisson system. The simulation is implemented on a classical emulator of a quantum computer using Qiskit [47], especially *statevector simulator* as the backend. This backend gives us access to the whole output space at all moments, and we do not implement QAE directly for saving the number of qubits. We compare the simulation results of the quantum algorithm using HS with those of a classical algorithm which have been obtained by directly solving the Vlasov equation and the Poisson equation using the Euler method for the time. These simulations are performed using the following parameters for a given wavenumber

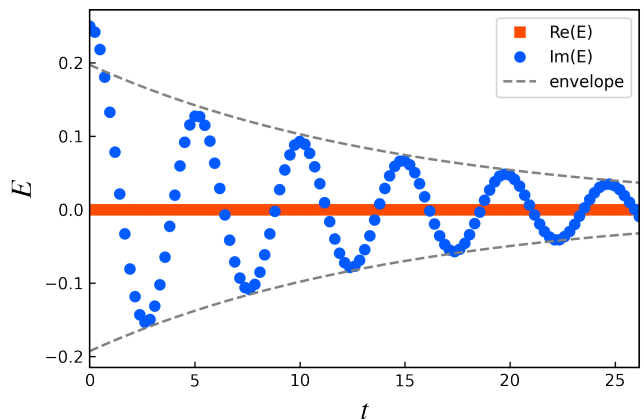


FIG. 13: Time evolution of the electric field E when using the quantum algorithm with $\Delta t = 0.238$ ($k = 0.4$). The envelope is a fitted exponential $\pm \exp(\gamma t)$.

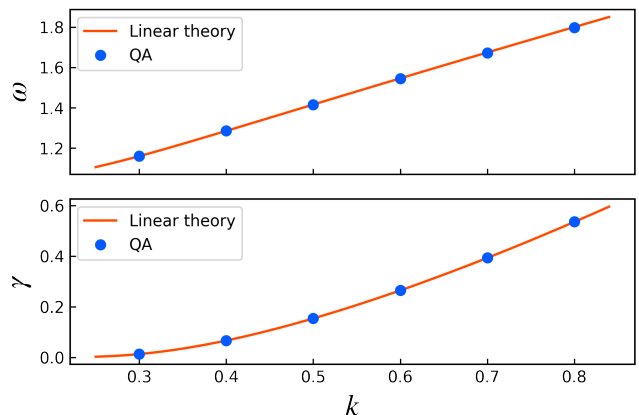


FIG. 14: Comparison of the frequencies and damping rates obtained from the results of the quantum algorithm (QA) for various wavenumbers with those obtained from the linear Landau theory.

k :

$$\begin{aligned} N_v &= 32, & f_M(v_j) &= \frac{1}{\sqrt{2\pi}} e^{-\frac{1}{2}v_j^2}, \\ v_{\max} &= 4.5, & f_1(v_j, t=0) &= 0.1f_M(v_j), \end{aligned} \quad (97)$$

$$E(t=0) = \frac{i}{k} \sum_j f_1(v_j, t=0) \Delta v.$$

We construct the unitary U' in Fig. 5 from the unitary $U = U_{\text{row}}^\dagger U_{\text{cal}}$ in Ref. [9], which is the $(\alpha, 4, 0)$ -block-encoding of H . Using the unitary U' , we construct the circuit U_{OAA} for $t = 2$ and choose an error tolerance $\varepsilon = 10^{-3}$. Then, U_{OAA} is a $(1, 7, 10^{-3})$ -block-encoding of $e^{-iH\Delta t}$, where $\Delta t = 1/\alpha$. We implement HS for the evolution time $l\Delta t$ using l sequential U_{HS} because it is difficult to compute the phases $\Phi^{(c)}$ and $\Phi^{(s)}$ for a large t as mentioned in Sec. III C.

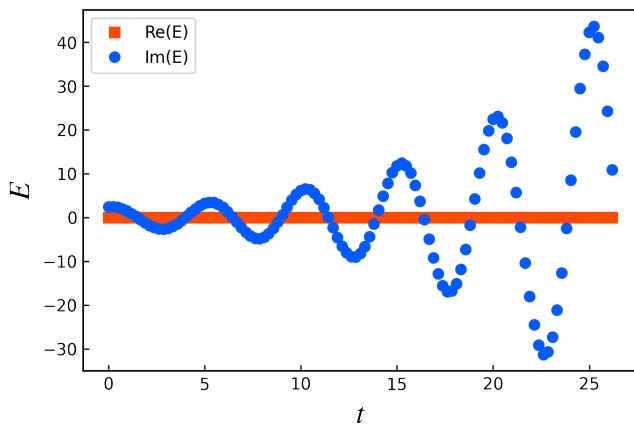


FIG. 15: Time evolution of the electric field E when using the classical algorithm using the Euler method with $\Delta t = 0.238$ ($k = 0.4$).

Figure 13 shows the time evolution of the electric field E for $k = 0.4$ using the quantum algorithm. In this case, the normalization of the Hamiltonian becomes $1/\alpha = 0.238$. After a brief initial stage, the imaginary component of E is damped and oscillating. We fit the curve with the function $Ae^{-i\gamma(t-t_0)} \cos(\omega(t-t_0) - \rho) + E_0$ to obtain parameters of interest, i.e., the frequency ω and damping rate γ :

$$\omega = 1.28508, \quad \gamma = 0.06623, \quad (98)$$

where $t_0 = 5.23$. One can find precise values of $\omega = 1.28506$ and $\gamma = 0.06613$ from the linear Landau theory [48]. Figure 14 shows the comparison of the frequencies and damping rates obtained from the results of the quantum algorithm with the linear theory for various wavenumbers. The parameters obtained by fitting the curves agree well with the linear theory. These results indicate that our quantum algorithm accurately reproduces the linear Landau damping. Hereafter, the case $k = 0.4$ is discussed in both the quantum and classical algorithms.

Figure 15 shows the time evolution of E with the same time step $\Delta t = 0.238$ in the classical algorithm using the Euler method. Unlike the quantum algorithm, the imaginary component of E diverges numerically because of the long time step. Table IV shows the relative errors of ω and γ for the quantum and classical algorithms with different time steps. The classical algorithm requires a smaller time step Δt to obtain ω and γ with the same order of accuracy as in the quantum algorithm.

In the linearized Vlasov-Poisson system, the energy transfer between the particles and the electric field occurs, and the distribution functions have a wavy structure. Figure 16 shows the velocity profiles of the distribution functions at different times. The distribution functions at $t = 8.32, 16.65,$ and 24.97 have a wavy structure. At $t = 16.65$ and 24.97 , the structure appears mainly around the phase velocity $v_\phi = \omega/k = 3.213$. These

TABLE IV: Comparison of the frequencies and damping rates with different time steps obtained from the quantum algorithm (QA) and classical algorithm (CA) for $k = 0.4$.

	Time step Δt	Relative error [%]	
		frequency ω	damping rate γ
QA	2.38×10^{-1}	1.67×10^{-3}	1.60×10^{-1}
	1.00×10^{-2}	6.25×10^{-2}	1.24×10^1
CA	1.00×10^{-3}	8.77×10^{-3}	-1.12
	5.00×10^{-4}	5.52×10^{-3}	-4.92×10^{-1}
	1.00×10^{-4}	2.91×10^{-3}	6.51×10^{-3}

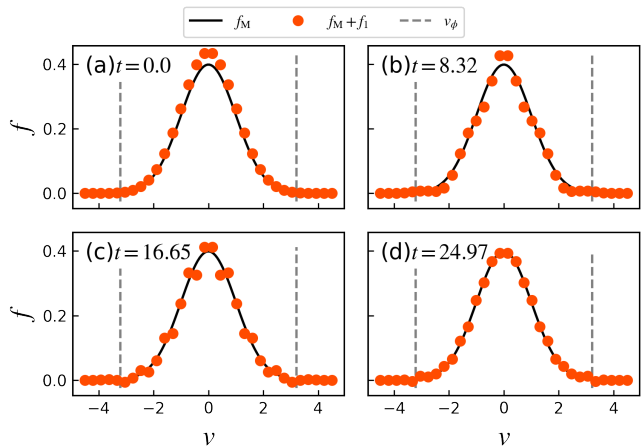


FIG. 16: Time evolution of the distribution function $f = f_M + f_1$ ($k = 0.4$). The solid black curve shows the Maxwellian $f = f_M$ distribution function. The gray dashed lines show the theoretical phase velocity $v_\phi = 3.21$.

results are consistent with the linear Landau theory [48].

We validate the results of the distribution functions by comparing them with those of the classical algorithm. The error between different distribution functions is defined as

$$\delta(f, g) = \sum_j |f_j - g_j|^2 \Delta v, \quad (99)$$

where f and g are different distribution functions. We denote f_{QA} and f_{CA} to the distribution functions obtained from the quantum algorithm (QA) and the classical algorithm (CA). The distribution function f_{CA} is corresponding to the case when $\Delta t = 1 \times 10^{-4}$ and $k = 0.4$. We consider the result of this case as accurate because the time step Δt is sufficiently small. Table V shows the errors between these distribution functions are sufficiently small. For reference, we show the error $\delta = 2.02 \times 10^{-5}$ between a Maxwellian distribution $f_M(v)$ and a drift-Maxwellian distribution $f_M(v - 10^{-4})$ for $N_v = 32$. These results indicate that our quantum algorithm can reproduce precisely the structure of the distribution function.

TABLE V: Errors between the distribution functions f_{QA} and f_{CA} , defined as in Eq. (99): f_{QA} is obtained from the quantum algorithm with $\Delta t = 0.238$ ($k = 0.4$); f_{CA} is obtained from the classical algorithm using the Euler method with $\Delta t = 1 \times 10^{-4}$ ($k = 0.4$).

t	δ [$\times 10^{-5}$]
0	0.000
8.32	0.560
16.65	0.925
24.97	1.06

VI. SUMMARY

In this study, we have shown how to apply the quantum singular value transformation (QSVT) to the Hamiltonian simulation (HS) algorithm and discussed the error and query complexity of HS using oblivious amplitude amplification (OAA) and fixed-point amplitude amplification (FPAA) within the QSVT framework. As a result, the number of queries for the OAA-based HS scales as $\mathcal{O}(t + \log(1/\varepsilon))$, whereas the FPAA-based one scales as $\mathcal{O}(t \log(1/\varepsilon) + \log^2(1/\varepsilon))$, where t is an evolution time and ε is an error tolerance. In addition, we have numerically compared the number of queries of these HS algorithms, showing that the number of queries of the OAA-based HS is smaller than that of the FPAA-based one, regardless of parameters t and ε . Fitting the curve of the plotted data, we computed the constant factors and coefficients hidden behind the asymptotic scaling. Then, we found that the values of OAA-based HS are smaller than those of FPAA-based HS. We also identified that the large number of queries of FPAA-based HS is due to the high degree required to approximate the sign function. Therefore, the OAA method is more appropriate for HS than the FPAA one.

Based on the above findings, applying OAA-based HS to the one-dimensional linearized Vlasov-Poisson system, we simulated the case of electrostatic Landau damping for various wavenumbers on a classical emulator of a quantum computer using Qiskit [47]. The frequencies ω and damping rates γ obtained by curve fitting the time evolutions of the electric field E are in agreement with the linear Landau theory [48]. Moreover, the velocity profiles of the distribution function f that the quantum algorithm produces match the classical ones for the same velocity grid size N_v . These results show that the quantum algorithm can reproduce precisely the linear Landau damping with the structure of the distribution function.

We have compared the results of the quantum algorithm using HS with those of the classical algorithm using the Euler method for time. The classical algorithm with a large time step $\Delta t = 0.238$ causes numerical divergence. On the other hand, the quantum algorithm remains stable for the same Δt . This stability is because the state at the next time can be analytically determined by $U = \exp(-iHt)$, which is one of the features of the

HS algorithm. The classical algorithm requires a smaller time step Δt to obtain ω and γ with the same order of accuracy as in the quantum algorithm. These results show that the HS algorithm has advantages in time step over the classical algorithm using the Euler method.

We have discussed the gate complexity of the algorithm for calculating the time evolution of the electric field E . The complexity scales logarithmically with the total grid size in velocity space N_v and linearly with the number of time steps N_t . We have proposed the algorithm for obtaining the deviation from the Maxwell distribution. The gate complexity of this algorithm also scales logarithmically with N_v . The circuits of the unitaries which are block-encodings of the Hamiltonian for the higher dimensional systems have been developed. The gate complexities of HS using the circuits can be represented in the same form as the one-dimensional system and scales logarithmically with N_v . This result indicates the quantum algorithm for the linearized Vlasov-Poisson system has exponential speedups over classical algorithms.

ACKNOWLEDGMENTS

This work is supported by MEXT Quantum Leap Flagship Program Grant Number JPMXS0118067285 and JPMXS0120319794, JSPS KAKENHI Grant Number 20H05966, and JST Grant Number JPMJPF2221.

Appendix A: From QSP to QSVT

Quantum singular value transformation (QSVT) is based on the results of quantum signal processing (QSP) [29]. QSP is performed using a series of two gates W and S defined as

$$W(x) \equiv e^{i \arccos(x)X} = \begin{bmatrix} x & i\sqrt{1-x^2} \\ i\sqrt{1-x^2} & x \end{bmatrix}, \quad (\text{A1})$$

for $x \in [-1, 1]$ and

$$S(\phi) \equiv e^{i\phi Z} = \begin{bmatrix} e^{i\phi} & 0 \\ 0 & e^{-i\phi} \end{bmatrix}. \quad (\text{A2})$$

These gates construct the following gate sequence

$$W_{\Phi'} \equiv e^{i\phi'_0 Z} \prod_{k=1}^d W(x) e^{i\phi'_k Z}, \quad (\text{A3})$$

where $\Phi' = (\phi'_0, \phi'_1, \dots, \phi'_d) \in \mathbb{R}^{d+1}$. This convention is called the Wx convention in Ref. [32].

Another convention is the Reflection convention, which uses a reflection gate R instead of W

$$R(x) \equiv \begin{bmatrix} x & \sqrt{1-x^2} \\ \sqrt{1-x^2} & -x \end{bmatrix}. \quad (\text{A4})$$

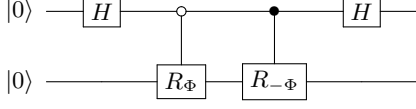


FIG. 17: Quantum circuit $U_{P_{\mathbb{R}}}$ that constructs a $(1, 1, 0)$ -block-encoding of $P_{\mathbb{R}}$.

The relationship between W and R is given by

$$W(x) = ie^{-i\frac{\pi}{4}Z} R(x) e^{-i\frac{\pi}{4}Z}. \quad (\text{A5})$$

Therefore, Eq. (A3) is rewritten as

$$\begin{aligned} e^{i\phi'_0 Z} \prod_{k=1}^d W(x) e^{i\phi'_k Z} &= e^{i\phi_0 Z} \prod_{k=1}^d R(x) e^{i\phi_k Z} \\ &\equiv R_{\Phi}, \end{aligned} \quad (\text{A6})$$

where

$$\begin{cases} \phi_0 = \phi'_0 + (2d-1)\frac{\pi}{4} \\ \phi_k = \phi'_k - \frac{\pi}{2} \quad (k=1, 2, \dots, d-1) \\ \phi_d = \phi'_d - \frac{\pi}{4}. \end{cases} \quad (\text{A7})$$

The phases $\Phi, \Phi' \in \mathbb{R}^{d+1}$ exist, and the gate sequence constructs the $(1, 1, 0)$ -block-encoding of a polynomial function $P \in \mathbb{C}$

$$\langle 0 | W_{\Phi'} | 0 \rangle = \langle 0 | R_{\Phi} | 0 \rangle = P(x), \quad (\text{A8})$$

if and only if the conditions (i)-(iv) in Sec. III hold. If $P_{\mathbb{R}}$ satisfies the conditions (v) and (vi) in Sec. III, then there exists $P \in \mathbb{C}$ that satisfies $\text{Re}(P) = P_{\mathbb{R}}$ and the above conditions (i)-(iv).

Since $R^*(x) = R(x)$, if the complex conjugate of R_{Φ} is taken, we can get

$$R_{\Phi}^* = e^{-i\phi_0 Z} \prod_{k=1}^d R(x) e^{-i\phi_k Z} = \begin{bmatrix} P^*(x) & \cdot \\ \cdot & \cdot \end{bmatrix}, \quad (\text{A9})$$

and R_{Φ}^* can be denoted as $R_{-\Phi}$. The quantum circuit in Fig. 17 constructs the $(1, 2, 0)$ -block-encoding of $P_{\mathbb{R}}$:

$$\begin{aligned} &\langle 0 | \langle 0 | U_{P_{\mathbb{R}}} | 0 \rangle | 0 \rangle \\ &= \langle + | \langle 0 | (|0\rangle \langle 0| \otimes R_{\Phi} + |1\rangle \langle 1| \otimes R_{-\Phi}) | + \rangle | 0 \rangle \\ &= \frac{P(x) + P^*(x)}{2} \\ &= P_{\mathbb{R}}(x). \end{aligned} \quad (\text{A10})$$

Now, we derive the result of QSVT from that of QSP. Suppose that U is a $(1, a, 0)$ -block-encoding of a matrix A such that $A = \sum_{k=1}^r \sigma_k |w_k\rangle \langle v_k|$. The unitaries U and $e^{i\phi\Pi}$, where $\Pi = 2|0\rangle_a \langle 0| - I$, act on the two-dimensional invariant subspaces $\text{Span}(|0\rangle_a |v_k\rangle, |\perp\rangle |v_k\rangle)$ and $\text{Span}(|0\rangle_a |w_k\rangle, |\perp\rangle |w_k\rangle)$,

where $|\perp\rangle$ satisfies $\langle \perp | 0 \rangle_a = 0$. The unitary U acts on these invariant subspaces as follows:

$$\begin{aligned} U |0\rangle_a |v_k\rangle &= \sigma_k |0\rangle_a |w_k\rangle + \sqrt{1 - \sigma_k^2} |\perp\rangle |w_k\rangle, \\ U |\perp\rangle |v_k\rangle &= \sqrt{1 - \sigma_k^2} |0\rangle_a |w_k\rangle - \sigma_k |\perp\rangle |w_k\rangle. \end{aligned} \quad (\text{A11})$$

Therefore, U becomes

$$\begin{aligned} U &= \sum_k \begin{bmatrix} \sigma_k & \sqrt{1 - \sigma_k^2} \\ \sqrt{1 - \sigma_k^2} & -\sigma_k \end{bmatrix} \otimes |w_k\rangle \langle v_k| \\ &= \sum_k R(\sigma_k) \otimes |w_k\rangle \langle v_k|, \end{aligned} \quad (\text{A12})$$

and U^\dagger becomes

$$\begin{aligned} U^\dagger &= \sum_k R^\dagger(\sigma_k) \otimes (|w_k\rangle \langle v_k|)^\dagger \\ &= \sum_k R(\sigma_k) \otimes |v_k\rangle \langle w_k|. \end{aligned} \quad (\text{A13})$$

Moreover, Π acts on the invariant subspaces as follows:

$$\begin{aligned} \Pi \otimes I_s &= (|0\rangle_a \langle 0| - |\perp\rangle \langle \perp|) \otimes \sum_k |w_k\rangle \langle v_k| \\ &= \sum_k \begin{bmatrix} 1 & 0 \\ 0 & -1 \end{bmatrix} \otimes |w_k\rangle \langle v_k| \\ &= \sum_k Z \otimes |w_k\rangle \langle v_k|. \end{aligned} \quad (\text{A14})$$

Therefore, $e^{i\phi\Pi}$ becomes

$$e^{i\phi\Pi} = \sum_k e^{i\phi Z} \otimes |w_k\rangle \langle v_k|. \quad (\text{A15})$$

Now, the alternating phase modulation sequence U_{Φ} defined in Eq. (7) becomes the $(1, a, 0)$ -block-encoding of $P^{(\text{SV})}(A)$ as for odd d :

$$\begin{aligned} U_{\Phi} &= \sum_k e^{i\phi_0 Z} \prod_{j=1}^d (R(\sigma_k) e^{i\phi_j Z}) \otimes |w_k\rangle \langle v_k| \\ &= \begin{bmatrix} \sum_k P(\sigma_k) |w_k\rangle \langle v_k| & \cdot \\ \cdot & \cdot \end{bmatrix} \\ &= \begin{bmatrix} P^{(\text{SV})}(A) & \cdot \\ \cdot & \cdot \end{bmatrix}, \end{aligned} \quad (\text{A16})$$

and for even d we can similarly derive. We can construct the $(1, a+1, 0)$ -block-encoding of the real polynomial function $P_{\mathbb{R}}^{(\text{SV})}$ like QSP. Since $U_{-\Phi}$ is the $(1, a, 0)$ -block-encoding of $P^{*(\text{SV})}$, we can construct a quantum

circuit $U_{\mathbb{R}}^{(SV)}$:

$$\begin{aligned}
& \langle 0|_b \langle 0|_a U_{\mathbb{R}}^{(SV)} |0\rangle_b |0\rangle_a \\
&= (\langle 0|_b H) \langle 0|_a (|0\rangle_b \langle 0| \otimes U_{\Phi} \\
&\quad + |1\rangle_b \langle 1| \otimes U_{-\Phi}) (H |0\rangle_b) |0\rangle_a \\
&= \frac{\langle 0|_a (U_{\Phi} + U_{-\Phi}) |0\rangle_a}{2} \\
&= \frac{P^{(SV)}(A) + P^{*(SV)}(A)}{2} \\
&= P_{\mathbb{R}}^{(SV)}(A). \tag{A17}
\end{aligned}$$

-
- [1] L. K. Grover, A fast quantum mechanical algorithm for database search, in *Proceedings of the twenty-eighth annual ACM symposium on Theory of computing* (ACM Press, New York, 1996) pp. 212–219.
- [2] P. W. Shor, Algorithms for quantum computation: discrete logarithms and factoring, in *Proceedings 35th Annual Symposium on Foundations of Computer Science* (IEEE Computer Society, USA, 1994) pp. 124–134.
- [3] A. W. Harrow, A. Hassidim, and S. Lloyd, Quantum algorithm for linear systems of equations, *Phys. Rev. Lett.* **103**, 150502 (2009).
- [4] A. M. Childs, R. Kothari, and R. D. Somma, Quantum algorithm for systems of linear equations with exponentially improved dependence on precision, *SIAM J. Comput.* **46**, 1920 (2017).
- [5] R. P. Feynman, Simulating physics with computers, *Int. J. Theor. Phys.* **21**, 467 (1982).
- [6] S. Lloyd, Universal quantum simulators, *Science* **273**, 1073 (1996).
- [7] F. Gaitan, Finding flows of a navier–stokes fluid through quantum computing, *Npj Quantum Inf.* **6**, 1 (2020).
- [8] F. Gaitan, Finding solutions of the navier-stokes equations through quantum computing—recent progress, a generalization, and next steps forward, *Adv. Quantum Technol.* **4**, 2100055 (2021).
- [9] A. Engel, G. Smith, and S. E. Parker, Quantum algorithm for the vlasov equation, *Phys. Rev. A* **100**, 062315 (2019).
- [10] I. Y. Dodin and E. A. Startsev, On applications of quantum computing to plasma simulations, *Phys. Plasmas* **28**, 092101 (2021).
- [11] I. Novikau, E. A. Startsev, and I. Y. Dodin, Quantum signal processing for simulating cold plasma waves, *Phys. Rev. A* **105**, 062444 (2022).
- [12] A. Ameri, P. Cappellaro, H. Krovi, N. F. Loureiro, and E. Ye, A quantum algorithm for the linear vlasov equation with collisions, arXiv:2303.03450 (2023).
- [13] Y. Cao, A. Papageorgiou, I. Petras, J. Traub, and S. Kais, Quantum algorithm and circuit design solving the poisson equation, *New J. Phys.* **15**, 013021 (2013).
- [14] S. Wang, Z. Wang, W. Li, L. Fan, Z. Wei, and Y. Gu, Quantum fast poisson solver: the algorithm and complete and modular circuit design, *Quantum Inf. Process.* **19**, 170 (2020).
- [15] P. C. S. Costa, S. Jordan, and A. Ostrander, Quantum algorithm for simulating the wave equation, *Phys. Rev. A* **99**, 012323 (2019).
- [16] A. Suau, G. Staffelbach, and H. Calandra, Practical quantum computing: Solving the wave equation using a quantum approach, *ACM Trans. Quantum Comput.* **2**, 1 (2021).
- [17] D. W. Berry, G. Ahokas, R. Cleve, and B. C. Sanders, Efficient quantum algorithms for simulating sparse hamiltonians, *Commun. Math. Phys.* **270**, 359 (2007).
- [18] A. M. Childs and R. Kothari, Limitations on the simulation of non-sparse hamiltonians, *Quantum Comput. Inf.* **10**, 669 (2010).
- [19] D. W. Berry and A. M. Childs, Black-box hamiltonian simulation and unitary implementation, *Quantum Inf. Comput.* **16**, 29 (2012).
- [20] A. M. Childs and N. Wiebe, Hamiltonian simulation using linear combinations of unitary operations, *Quantum Inf. Comput.* **12**, 901 (2012).
- [21] D. W. Berry, A. M. Childs, R. Cleve, R. Kothari, and R. D. Somma, Exponential improvement in precision for simulating sparse hamiltonians, in *Proceedings of the forty-sixth annual ACM symposium on Theory of computing* (ACM Press, New York, 2014) pp. 283–292.
- [22] D. W. Berry, A. M. Childs, and R. Kothari, Hamiltonian simulation with nearly optimal dependence on all parameters, in *2015 IEEE 56th annual symposium on foundations of computer science* (IEEE Computer Society, USA, 2015) pp. 792–809.
- [23] D. W. Berry, A. M. Childs, R. Cleve, R. Kothari, and R. D. Somma, Simulating hamiltonian dynamics with a truncated taylor series, *Phys. Rev. Lett.* **114**, 090502 (2015).
- [24] D. W. Berry and L. Novo, Corrected quantum walk for optimal hamiltonian simulation, *Quantum Inf. Comput.* **16**, 1295 (2016).
- [25] L. Novo and D. W. Berry, Improved hamiltonian simulation via a truncated taylor series and corrections, *Quantum Inf. Comput.* **17**, 623 (2017).
- [26] A. M. Childs, D. Maslov, Y. Nam, N. J. Ross, and Y. Su, Toward the first quantum simulation with quantum speedup, *Proc. Natl. Acad. Sci. U.S.A.* **115**, 9456 (2018).
- [27] G. H. Low and I. L. Chuang, Optimal hamiltonian simulation by quantum signal processing, *Phys. Rev. Lett.* **118**, 010501 (2017).

- [28] G. H. Low and I. L. Chuang, Hamiltonian simulation by qubitization, *Quantum* **3**, 163 (2019).
- [29] A. Gilyén, Y. Su, G. H. Low, and N. Wiebe, Quantum singular value transformation and beyond: exponential improvements for quantum matrix arithmetics, in *Proceedings of the 51st Annual ACM SIGACT Symposium on Theory of Computing* (ACM Press, New York, 2019) pp. 193–204.
- [30] M. A. Nielsen and I. L. Chuang, *Quantum Computation and Quantum Information* (American Association of Physics Teachers, 2010).
- [31] M. Szegedy, Quantum speed-up of markov chain based algorithms, in *45th Annual IEEE symposium on foundations of computer science* (IEEE Computer Society, USA, 2004) pp. 32–41.
- [32] J. M. Martyn, Z. M. Rossi, A. K. Tan, and I. L. Chuang, Grand unification of quantum algorithms, *PRX Quantum* **2**, 040203 (2021).
- [33] A. Paetznick and K. M. Svore, Repeat-until-success: Non-deterministic decomposition of single-qubit unitaries, *Quantum Inf. Comput.* **14**, 1277 (2014).
- [34] A. Daskin and S. Kais, An ancilla-based quantum simulation framework for non-unitary matrices, *Quantum Inf. Process.* **16**, 1 (2017).
- [35] L. K. Grover, Fixed-point quantum search, *Phys. Rev. Lett.* **95**, 150501 (2005).
- [36] T. Tulsi, L. K. Grover, and A. Patel, A new algorithm for fixed point quantum search, *Quantum Inf. Comput.* **6**, 483 (2006).
- [37] T. J. Yoder, G. H. Low, and I. L. Chuang, Fixed-point quantum search with an optimal number of queries, *Phys. Rev. Lett.* **113**, 210501 (2014).
- [38] G. Brassard, P. Høyer, M. Mosca, and A. Tapp, Quantum amplitude amplification and estimation, *Quantum Comput. Inf.* **305**, 53 (2002).
- [39] G. H. Low, T. J. Yoder, and I. L. Chuang, Methodology of resonant equiangular composite quantum gates, *Phys. Rev. X* **6**, 041067 (2016).
- [40] G. H. Low and I. L. Chuang, Hamiltonian simulation by uniform spectral amplification, arXiv:1707.05391 (2020).
- [41] R. Chao, D. Ding, A. Gilyén, C. Huang, and M. Szegedy, Finding angles for quantum signal processing with machine precision, arXiv:2003.02831 (2020).
- [42] R. Chao, D. Ding, A. Gilyén, C. Huang, and M. Szegedy, Finding angles for quantum signal processing with machine precision (2021), <https://github.com/ichuang/pyqsp>, accessed: 07/2022.
- [43] G. H. Low, *Quantum signal processing by single-qubit dynamics*, Ph.d. thesis, Massachusetts Institute of Technology (2017).
- [44] K. Mitarai and W. Mizukami, Perturbation theory with quantum signal processing, arXiv:2210.00718 (2022).
- [45] A. Prakash, *Quantum algorithms for linear algebra and machine learning* (University of California, Berkeley, 2014).
- [46] V. Giovannetti, S. Lloyd, and L. Maccone, Architectures for a quantum random access memory, *Phys. Rev. A* **78**, 052310 (2008).
- [47] M. S. A. *et al.*, Qiskit: An open-source framework for quantum computing (2021).
- [48] F. F. Chen, *Introduction to plasma physics and controlled fusion* (Springer, New York, 1984) pp. 224–232.